Helsinki University of Technology

Department of Electrical and Communications Engineering

Optoelectronics laboratory

Computational methods for finite thickness photonic crystals

Karri Varis

Dissertation for the degree of Doctor of Science in Technology to be presented with due permission of the Department of Electrical and Communications Engineering, for public examination and debate in Auditorium S4 at Helsinki University of Technology (Espoo, Finland) on the 2nd of December, 2005, at 12 o'clock noon.

Espoo, Finland
2005

Distribution:
Helsinki University of Technology
Department of Electrical and Communications Engineering
Optoelectronics Laboratory
P.O. Box 3500
FIN-02015 HUT
FINLAND
This dissertation can be read at http://lib.tkk.fi/Diss/

ISBN 951-22-7937-1 (printed version)
ISBN 951-22-7938-X (electronic version)

Painotalo

Abstract

We develop a computational algorithm for finite thickness photonic crystals and apply it to photonic crystal slabs and artificial opals. The algorithm is not limited to solving only photonic crystals but can be applied to any electromagnetic problem, which is periodic in a plane and has a finite thickness in the perpendicular direction. An application in cylindrical coordinates is also presented. The method is based on the diagonalized form of Maxwell's equations, in which one spatial direction is distinguished and isolated. We show that this formulation is especially suitable for problems, which are periodic along two and non-periodic along the third axis. The fields are expanded in a combination of several bases, planewaves in the transversal plane, finite differences and eigenvectors in the perpendicular direction. The method is applied to both eigenmode and excitation problems. Furthermore, we develop an efficient scheme for computing the reflection of arbitrarily shaped and polarised beams from the surface of a periodic media. A great emphasis is laid on accuracy and efficiency. The resulting equations are solved using iterative techniques together with problem adapted, operator level preconditioners. Finally, we compare the computations to measurement results obtained from artificial opals.

Preface

This work consists of an overview and four publications listed separately. The work was done in Optoelectronics Laboratory of Helsinki University of Technology between years 1999 and 2005 together with two intensive periods in Vienna University of Technology in 2001 and 2003.

I want to express my gratitude to Professors Turkka Tuomi and Harri Lipsanen for giving me the opportunity to work in Optoelectronics Laboratory and for their continuous support during this time. I also thank Dr. Markku Sopanen for his invaluable advice and pleasant company over the years.

I am very grateful for the support provided by Dr. Juha Toivonen and M.Sc. Lauri Knuuttila. Our numerous innovation meetings over the years have been a major source of new ideas for me. The adventures we have gone through together have certainly taught me many things and furthermore, they have been very entertaining.

I want to thank M.Sc. Sanna Arpiainen and M.Sc. Marco Mattila for providing me with useful data and their advice in analysing it. I thank M.Sc. Anu Huttunen for our joint efforts in solving the mysteries of photons in crystalline materials. I am in great debt to M.Sc. Aapo Lankinen for our fruitful discussions and the advice he has given me. I also want to express my gratitude to all other colleagues, current and past, who are unfortunately too numerous to be mentioned here by name.

Most of all, I am very grateful to Professor Ali R. Baghai-Wadji from Vienna University of Technology for his great support, continuous supply of excellent new ideas, the education he has provided me with and the wonderful possibility to join his research group in Vienna.

I greatly acknowledge my brother Markku for the great company he has been during these years. I also want to express my sincere gratitude to my parents for the support they have given me and the interest they have shown in my work. Finally, I am immensely grateful to my fiancée Ulla, who has had the patience to put up with me and my research all these years.

Espoo, April 2005

Karri Varis

List of publications

I K. Varis, A. R. Baghai-Wadji, "*A 2D Pseudo-Spectral Approach of Photonic Crystal Slabs*," ACES Journal, **20**, 107-118 (2005)

II K. Varis, A. R. Baghai-Wadji, "*A Novel 3D Pseudo-Spectral Analysis of Photonic Crystal Slabs*," ACES Journal, **19**, 101-111 (2004).

III K. Varis, A. R. Baghai-Wadji, "*Pseudo-spectral Analysis of Radially-Diagonalized Maxwell's Equations in Cylindrical Co-ordinates*," Optics Express, **11**, 3048-3062 (2003).

IV K. Varis, M. Mattila, S. Arpiainen, J. Ahopelto, F. Jonsson, C. M. Sotomayor Torres, M. Egen, R. Zentel, "*Reflection of focused beams from opal photonic crystals*," Optics Express, **13**, 2653-2667 (2005).

Author's contribution

The author has written and done the research in articles I, II and III in collaboration with Professor A. R. Baghai-Wadji. The author has written and performed the theoretical work in article IV. All research related to linear algebra and computation in all articles was done by the author.

The articles are ordered to reflect the course of the work instead of the publication date. The author believes that this is a more logical order and makes the book easier to follow for the reader.

Notations used in this book

We use the following conventions throughout this book. Other conventions are frequently used in the attached publications but their meaning is made clear in the context.

$\mathcal{A}$	Calligraph font, a differential operator or operator matrix.
∂_x	Partial derivation operator with respect to x.
$\mathbf{\Psi}$	Uppercase Greek letter, a hypervector whose elements may be functions, components of physical vectors or algebraic vectors of expansion coefficients for those.
$\vec{k}$	Lower case font with an arrow on top. A physical vector, such as a wave vector or a lattice vector.
k_x	The x-directional component of the physical vector $\vec{k}$.
$\mathbf{A}$	Upper case bold font, matrix. Especially, if $\mathcal{A}$ is differential (matrix) operator, then $\mathbf{A}$ is its discretized representation.
$\mathrm{diag}(\mathbf{A})$	Diagonal elements of $\mathbf{A}$.
$\mathbf{I}$	An eye matrix.
$\mathbf{e}$	Lower case bold font, an algebraic vector. Especially, a vector of expansion coefficients.
e_n	An individual element of a coefficient vector $\mathbf{e}$.
$\vec{u}_x$	A dimensionless unit vector in the direction x.
$f^{(i)}$	If $f(z)$ is a function of z, then $f^{(i)}$ denotes f evaluated at z_i.
j	The imaginary unit.
$O(\cdot)$	An asymptotic bound

Contents

1 Introduction **1**
- 1.1 Different kinds of photonic crystals . . . 2
- 1.2 Computational methods for photonic crystals . . . 4
- 1.3 Overview of text . . . 5

2 Basic concepts **6**
- 2.1 A generalized photonic crystal slab . . . 6
- 2.2 Bands and bandgaps . . . 6
- 2.3 Diagonalized form . . . 8

3 Properties of Maxwell's equations **9**
- 3.1 Diagonalization of Maxwell's equations . . . 9
- 3.2 Eigenvalues and vectors . . . 10
- 3.3 Solving the slab modes in terms of eigenvectors . . . 12

4 Algorithm for photonic crystal slabs **14**
- 4.1 Planewave expansion . . . 14
- 4.2 Finite difference discretization . . . 14
- 4.3 Eigenvector expansion in the claddings . . . 16
- 4.4 Matching the interface conditions . . . 18
- 4.5 Putting it all together . . . 19

5 Algorithm for cylindrical coordinates **20**
- 5.1 Boundary conditions in cylindrical coordinates . . . 21

6 Solving the equation system **23**
- 6.1 Solving the bands . . . 23
- 6.2 Current excitations . . . 24
- 6.3 Scattering problems . . . 26

7 Iterative techniques **27**
- 7.1 Preconditioning . . . 28
- 7.2 The Jacobi preconditioner . . . 28
- 7.3 The auxiliary problem preconditioner . . . 29
- 7.4 The block diagonal preconditioner . . . 29
- 7.5 The two-sided preconditioner . . . 30

8 Artificial opals **32**
- 8.1 Reflection of beams from opals . . . 32
- 8.2 Comparison to experimental results . . . 35

9 Discussion **37**

10 Outlook **38**

Bibliography **39**

1 Introduction

Modern electronics has become a part of our everyday life but few people stop to think that this is only possible because quantum mechanics was developed during the last century. To understand how a microprocessor works is subject to understanding how electrons behave in crystalline semiconductor materials. Within the realm of classical physics, where electrons are considered to be solid particles, this is impossible but in 1920's Louis de Broglie suggested that electrons could also be treated as waves [1], the so called probability waves. These are not waves in a common sense because instead of describing the particle itself, they describe probabilities where and when the particle might be found. In any case, waves are the only way to explain the interaction of electrons with the periodic lattice of atoms in semiconductors. Especially, the concepts of bands and bandgaps, which are behind the inventions like diodes and semiconductor lasers, become understandable when the wave picture is used.

Since light has been known to have the wave property long before electrons, it is reasonable to ask if optical crystals exist as well and whether they would resemble their atomic counterparts. The answer is yes, optical crystals, or photonic crystals as they are more often called, do indeed exist and light has the most unusual behaviour in them. Unlike semiconductors, where the electrons interact with the periodic potential produced by the lattice of atoms (and other electrons, to be precise), photonic crystals are based on the periodic variation of the refractive index.

To get an example of a photonic crystal, consider a simple and well known structure called a quarter wave stack, which is made by piling two dielectric layers of different widths and refractive indices periodically on top of each other [2]. Light incident on the stack will reflect according to Snell's law from each of the dielectric interfaces but if the wavelength of light happens to be four times longer than the optical thickness of each layer, then all the reflected waves have the same phase and add coherently. The consequence is that the reflectance of the stack will approach 100% for resonant wavelengths, even if the reflectance of an individual interface is low. The anti-resonant wavelengths, on the other hand, behave in the opposite way and are not reflected by the stack at all. In fact, it is not only the resonant wavelength but a whole range of wavelengths, denoted the photonic bandgap, which are completely reflected by the stack. The quarter wave stack is often used as a wavelength selective, high quality mirror but it has one problem: if the light is not incident perpendicularly, the optical thicknesses of the layers change and the bandgap occurs for different wavelengths. Something more advanced, which can account for the direction of the light, is obviously needed.

In 1990, Ho *et al*. [3] theoretically predicted that it is possibly to create a three dimensional lattice of dielectric "atoms" such that for a certain wavelength range, there will be an optical bandgap for all directions simultaneously. This phenomenon, referred to as a complete photonic bandgap, is probably the most interesting of all the peculiar effects that a photonic crystal may have on light. To give an example of applications, consider a photonic crystal with one "atom" removed from

an otherwise perfect lattice. In suitable circumstances, it may happen that light whose wavelength is in the bandgap, can exist around the missing "atom" but nowhere else in the crystal. In other words, light gets trapped because it simply cannot go anywhere else. The point-defect concept has been used to create minuscule lasers [4] and it has also very interesting applications in basic research [5]. A similar phenomenon has also been used for making waveguides: if a whole row of "atoms" is removed or disturbed, a certain wavelength of light may be allowed to propagate along the channel so created but not escape it [6]. The attraction is that photonic crystal waveguides have a potential of guiding light around sharp bends without loss, something which is beyond the capabilities of traditional dielectric waveguides.

There are some widely known examples of photonic crystals in the nature, even though not many people are aware of the underlying crystalline features. Most notably, the gemstone opal, which is produced by geological processes in the core of earth, is actually a cubic close packed (CCP) lattice of silica spheres [7]. The iridescent colors of opals are a result of a coherent scattering from the optical structure, as opposed to conventional colors, which are usually produced by the atomic properties of materials. Quite recently it has been discovered that there are also numerous examples of photonic crystals in biology [8, 9]. The glittering colors in some birds and butterflies are produced by a subwavelength microstructure and similar effects are also found in many other species in flora and fauna. Common examples include some hummingbird and peacock species. Some insects have even adopted an opposite strategy and use photonic crystal effects to produce anti-reflection coatings for camouflage [10].

The recent interest in photonic crystals can be largely addressed to the advances in the manufacturing technology, which has allowed scientists to create and investigate artificial photonic crystals in laboratories (see e.g. [11, 12] and references therein). However, the fabrication technique is still very difficult and a lot of work remains to be done before the process becomes routine. In order to get an impression of the challenges, consider a photonic crystal tuned to operate at a near infrared wavelength 1550 nm, which is often used in telecommunication applications. According to the band diagram presented in Ref. [13], the distance between the neighbouring "atoms" should be 550 nm. The separation between two distinct details 190 nm and the fabrication tolerances still much less. Undoubtedly, it is not a trivial task to make such a structure.

1.1 Different kinds of photonic crystals

Several methods for making three dimensional (3D) crystals have been tried during the past years. Examples of these are the Yablonovite [13], the woodpile structure [14, 15] and crystals made by micro-machining [16]. Unfortunately, none of these produce really satisfying results or are too complicated to be applied in a large scale. A much simpler approach is to take advantage of the self organizing property of dielectric spheres in a suspension and create artificial opals [17–19]. This method has indeed resulted in some very good quality crystals (see e.g. paper IV) but the problem is that introducing purposeful defects, which actually make the photonic crystals interesting, is very challenging.

The difficulty in making 3D crystals has lead scientists to consider easier alternatives, some of

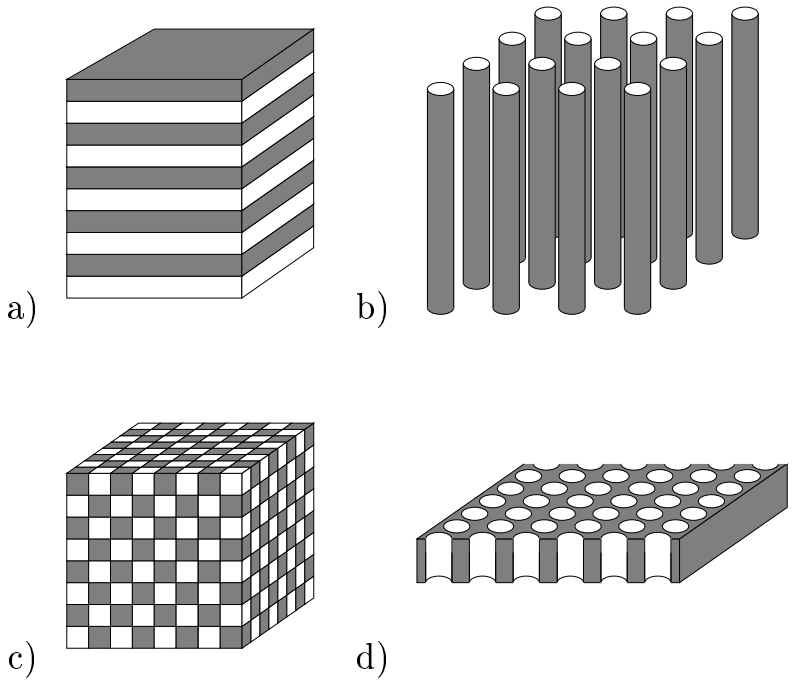

Figure 1.1: A schematic representation of different types of photonic crystals. a) A quarter wave stack or a 1D photonic crystal, which is composed by stacking infinitely large but finite thickness layers of top of each other. b) A 2D crystal made of a lattice of infinitely long dielectric rods. c) A 3D crystal, which is periodic along all three coordinate axes. d) A photonic crystal slab consisting of a periodic lattice of air holes embedded in a thin dielectric slab.

which are shown in Fig. 1.1. The simplest of them is a two dimensional (2D) photonic crystal (see e.g. [20] and references therein), which is periodic only along two axes and is assumed to be constant and infinite along the third. As long as the whole world is considered two dimensional, the 2D crystals have very similar theoretical properties with the 3D crystals. Unfortunately, we live in a three dimensional world and problems will arise since there is nothing to prevent the light from scattering in the vertical direction. This leads to a shift in the bandgap, quite as it happens in the quarter wave stack.

The third candidate and the main topic of this work is a photonic crystal slab [21–23], which builds on the ideas of 2D crystals but offers a way to control the vertical scattering[1]. A photonic crystal slab is essentially a 2D crystal, which is embedded in a thin dielectric slab, surrounded by lower refractive index material on both sides. The purpose of the slab is to act as a traditional dielectric waveguide and thereby discretize the optical mode spectrum in the perpendicular direction. This

[1]Many authors do not separate between 2D crystals and photonic crystal slabs but confusingly call them both 2D photonic crystals. Since they are inherently different things, we will distinguish between the two.

gives means to analyse, control and limit the vertical scattering but unfortunately, not prevent it completely. Particularly, the realization of a lossless point defect is impossible because there will always be coupling to the vacuum states in the claddings. Photonic crystal slabs are similar to 2D crystals in many respects but there are also some significant differences. The optical fields do not (generally) split to pure polarisations as they do in two dimensional systems and the scattering mechanism is also quite different. However, photonic crystal slabs show many properties one would expect in real crystals and the fact that they can be manufactured relatively easily, makes them attractive candidates for several applications in photonics.

1.2 Computational methods for photonic crystals

A host of different algorithms for simulating photonic crystals have been developed. Perhaps the most common of these is the planewave method (PWM), in which one expands the optical fields in terms of planewaves and then minimizes some functional in order to find the eigenstates of the crystal [3]. While this method is very powerful, it also has some drawbacks. The planewave basis tacitly implies the geometry to be periodic, which is fine for 2D and 3D crystals but is very cumbersome for finite thickness structures, such as the photonic crystal slab. The planewave method can be applied for analysing the guided modes in slab problems if the slab is surrounded by a thick layer of empty space. Then it does not matter whether the geometry is periodic or not because the adjacent slabs are so far away from each other that the optical fields in them are decoupled anyway (the so called supercell method [24]). This procedure is, however, not very efficient because one ends up simulating a vast area of empty space, where nothing interesting happens.

A quite different approach is the Finite-Difference Time-Domain (FDTD) method [25], which does not use the time harmonic assumption and is therefore well adapted to dynamic and transient problems [26]. Photonic bands can also be computed by simulating the evolution of some, possibly random, initial field and then Fourier transforming the resulting time series [27]. However, this process is not guaranteed to find all the eigenfrequencies and the extraction of the eigenfunctions requires a new simulation for each one of them. In problems where eigenfrequencies are not the main issue, such as waveguide bends [28] or cavity losses [29], FDTD is often the preferred choice.

An appealing method for solving photonic crystal slab problems is the transfer matrix method (TMM), which has a great number of different implementations. A common factor in all of them is that a matrix, which relates the fields on one boundary to those on another is somehow created. The fields can be expanded in terms of finite differences or finite elements [30], planewaves [31], eigenvectors [32] or even in some other basis. The advantages include that one can relatively easily compute dispersion relations and reflection or transmission coefficients of the structure. This approach is also suitable for frequency dependent dielectrics. The problem with most TMM implementations is that they are known to suffer from numerical instabilities [32].

Yet another promising technique for photonic crystal computations is the multiple scattering method, which is very versatile and can be applied on 2D [33, 34] and 3D [35] crystals, both

infinitely large and finite sized. The idea is to expand the scattering matrix of individual scatterers in terms of spherical (3D) or cylindrical (2D) harmonics and then compute the scattering matrix of the whole crystal using the Graf's addition theorem. Computation can be done very efficiently provided that the scattering matrices of the lattice elements are known analytically, which is the case for spherical and cylindrical particles. The multiple scattering method requires all particles, no matter what their shape is, to be enclosed by non-overlapping spheres (3D) or circles (2D). This means that the properties of e.g. a closed packed lattice of elliptical particles cannot be solved.

In this work, we develop a method for finite thickness photonics crystals, including but not limited to photonic crystal slabs. The method is related to both the planewave method and the transfer matrix method but has its own unique features, which make it particularly efficient on a class of problems that are periodic along two axes and non-periodic along the third. Our approach is to divide the slab into thin layers and expand the fields in them using planewaves. The planewave expansions on adjacent layers are then related to each other using finite differences in Fourier space. Above and below the slab, we expand the fields in terms of homogeneous-medium eigenvectors, which can be computed analytically. Finally, an equation from which the fields can be solved is created by applying interface conditions between the three domains. Our strategy is to discretize and solve the optical field explicitly inside the whole volume of the slab, as opposed to most transfer matrix methods where the unknowns inside the slab are eliminated and only the fields on the interfaces enter the final equation. Our approach leads to a matrix, which is much bigger than in TMM but on the other hand, it is very sparse and can be constructed with little computational effort. Efficient preconditioners will also be developed allowing the resulting matrix equation to be solved quickly using iterative techniques. We also briefly consider two possible implementations of the transfer matrix method but find them to be inefficient and unstable. Finally, our approach is applied to 2D and 3D slabs and to one dimensionally periodic problems, which are expressed in cylindrical coordinates.

1.3 Overview of text

The aim of this text is to give a unified representation of the publications included in this thesis. The focus is mainly on theoretical and numerical considerations, but the accuracy of the developed method is also verified by a comparison to measurement data from artificial opals. On selected topics, we give more detailed information than was possible to include in the articles. We will also review some previously unpublished but unfruitful efforts so that others can learn from our mistakes.

The text is organized as follows: We begin by defining some basic concepts necessary for understanding photonic crystals in chapter 2. Chapter 3 is devoted to analysing the diagonalized form of the Maxwell's equations and a computational algorithm based on the findings is developed in chapter 4. A modification of the algorithm for cylindrical coordinates is discussed in chapter 5. In chapters 6 and 7 we concentrate on numerical techniques for solving the related equations efficiently. The method is verified with a comparison to measurement data in chapter 8. Finally, the discussion is summarized in chapter 9 and a future outlook is given in chapter 10.

2 Basic concepts

In this chapter, we discuss and define some basic concepts that are necessary for understanding the remainder of the text.

2.1 A generalized photonic crystal slab

Conventionally, slabs in optics are considered to be thin and homogeneous dielectric layers, which are often used for guiding light. A photonic crystal slab is a modification of a conventional slab, in which the dielectric function is made periodic in the plane of the slab but is assumed to be homogeneous throughout the slab thickness. In this work, we consider generalized photonic crystal slabs, where the dielectric function is also allowed to vary along the slab thickness. Mathematically, the geometry is defined by

$$\varepsilon(\vec{r},z) = \begin{cases} \varepsilon_{\mathrm{a}}, & z > h \\ \varepsilon_{\mathrm{b}}(\vec{r},z), & 0 \le z \le h \\ \varepsilon_{\mathrm{c}}, & z < 0 \end{cases}, \tag{2.1}$$

where ε_{a} and ε_{c} are constants and ε_{b} satisfies the periodicity relation $\varepsilon_{\mathrm{b}}(\vec{r}+\vec{a},z) = \varepsilon_{\mathrm{b}}(\vec{r},z)$ for any vector $\vec{a} = m\vec{a}_1 + n\vec{a}_2$, with m and n being integers. The lattice vectors $\vec{a}_1$ and $\vec{a}_2$ obey the following relations: *i*) $\vec{a}_1 \cdot \vec{u}_z = \vec{a}_2 \cdot \vec{u}_z = 0$ (both lattice vectors lie on xy-plane) and *ii*) $\vec{a}_1 \times \vec{a}_2 \neq \vec{0}$ (lattice vectors are not zero vectors or parallel to each other).

We will also briefly discuss problems where either ε_{a} or ε_{b} or both satisfy the following requirements: *i*) $\varepsilon(\vec{r}+\vec{a},z) = \varepsilon(\vec{r},z)$ (share the periodicity with the slab) and *ii*) $\partial_z \varepsilon \equiv 0$ (are invariant in the z-direction).

2.2 Bands and bandgaps

In homogeneous-space, the wave vector $\vec{k}$ and the angular frequency ω of the radiation are related through a simple dispersion relation

$$\omega = \frac{c}{\sqrt{\varepsilon_{\mathrm{r}}}}|\vec{k}|, \tag{2.2}$$

where c is the vacuum speed of light and ε_{r} is the relative dielectric constant of the underlying medium. If the dielectric constant is replaced by a periodic function

$$\varepsilon_{\mathrm{r}}(\vec{r}) = \varepsilon_{\mathrm{r}}(\vec{r}+\vec{a}), \tag{2.3}$$

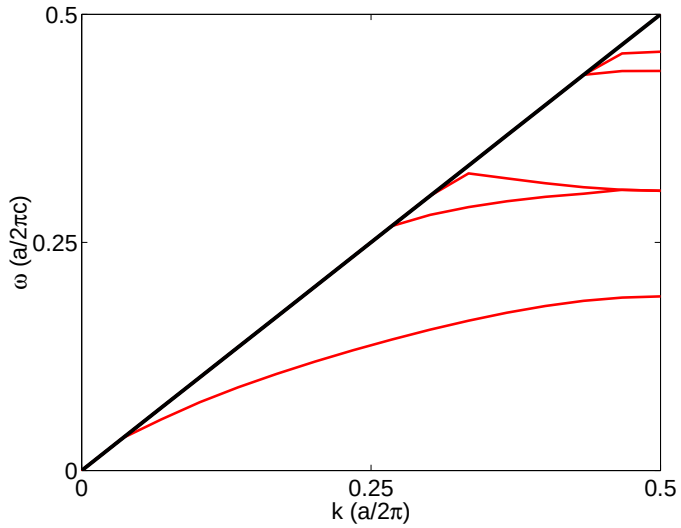

Figure 2.1: Dispersion diagram of TE-polarised modes in a corrugated waveguide [37]. The period of the waveguide along the x-direction is a, thickness is $0.7a$, the corrugation length is $0.5a$ and the slab is assumed to be infinitely thick in the y-direction. The relative dielectric constant in the slab is $\varepsilon = 13$, the material in the corrugation and above and below the slab is air.

where $\vec{r}$ is the position vector and $\vec{a} = n_1\vec{a}_1 + n_2\vec{a}_2 + n_3\vec{a}_3$ is any lattice vector, the dispersion relation obtains the form

$$\omega = f(\vec{k}), \tag{2.4}$$

where f is some function determined by the details of $\varepsilon_r(\vec{r})$. Based on the general knowledge of periodic systems (particularly quantum mechanics, see e.g. [36]), we can draw a few conclusions on f: *i*) It is periodic, $f(\vec{k}+\vec{g}) = f(\vec{k})$, where $\vec{g} = m_1\vec{g}_1 + m_2\vec{g}_2 + m_3\vec{g}_3$, with m_1, m_2 and m_3 being integers, is some reciprocal lattice vector related to the real space lattice by the equation

$$\vec{g}_1 = 2\pi\frac{\vec{a}_2 \times \vec{a}_3}{\vec{a}_1 \cdot (\vec{a}_2 \times \vec{a}_3)} \tag{2.5}$$

and cyclic permutations. *ii*) It may have several solutions ω_n corresponding to the same wave vector (and its periodic counterparts) and *iii*) each solution ω_n is continuous and differentiable in $\vec{k}$.

In the remainder of this text, functions $\omega_n(\vec{k})$ are called bands. Furthermore, a plot of all or some bands is called a band diagram. A band diagram is typically limited to the first irreducible Brillouin zone, i.e. for the smallest set of different values of $\vec{k}$ for which $\omega(\vec{k})$ is not degenerate based on translation, rotation or inversion symmetry of the lattice. An example of a band diagram is shown in Fig. 2.1.

Given a suitable dielectric function $\varepsilon_r(\vec{r})$, it may happen that the mapping $\vec{k} = \vec{f}^{-1}(\omega)$ does not exist for real valued ω and $\vec{k}$ on some interval $\omega \in [\omega_{low}, \omega_{high}]$. This interval is called the photonic bandgap.

2.3 Diagonalized form

Let us distinguish one direction in space and denote it $\vec{v}$. The plane perpendicular to $\vec{v}$ is called S. A differential equation is said to be diagonalized with respect to $\vec{v}$ [38], if it is written in the form

$$\mathcal{L}_S \Psi_S = \partial_{\vec{v}} \Psi_S, \tag{2.6}$$

where $\mathcal{L}_S$ is a linear differential operator operating on S and $\partial_{\vec{v}}$ is a derivative operator in the direction of $\vec{v}$. The vector field Ψ_S includes those components of the underlying physical vector field, which are tangential to S. In the following, we refer to Ψ_S as the transversal field and assume it to be at least piecewise differentiable on S and in $\vec{v}$.

The diagonalized form in Eq. (2.6) has a number of distinct properties:

1. If the transversal field Ψ_S is known on some plane S, its normal derivative can be computed using $\mathcal{L}_S$.

2. Interface conditions on S enter automatically into Eq. (2.6) because only the transversal field components are included in Ψ_S.

3. If Ψ_S is known to an arbitrary precision on a domain where it is n-times differentiable, then its normal derivatives can be computed up to the nth order using Eq. (2.6). To show this, apply $\mathcal{L}_S$ to both sides of Eq. (2.6) and interchange the order of $\partial_{\vec{v}}$ and $\mathcal{L}_S$ on the right hand side to give $\mathcal{L}_S \mathcal{L}_S \Psi_S = \partial_{\vec{v}} (\mathcal{L}_S \Psi_S)$. Denote $\mathcal{L}_S^2 = \mathcal{L}_S \mathcal{L}_S$ and substitute Eq. (2.6) to the right hand side, which gives $\mathcal{L}_S^2 \Psi_S = \partial_{\vec{v}}^2 \Psi_S$. A simple proof by induction shows that $\mathcal{L}_S^n \Psi_S = \partial_{\vec{v}}^n \Psi_S$.

4. If Ψ_S is known to an arbitrary precision on some plane S and the space is homogeneous in $\vec{v}$, we can compute the field on any parallel plane $S+\Delta$ using a Taylor expansion
$$\Psi_{S+\Delta} = \sum_n \frac{\Delta^n}{n!} \mathcal{L}_S^n \Psi_S. \tag{2.7}$$

5. If the space has a discontinuity on some plane $S+\Delta$, we can use Eq. (2.7) for computing the transversal field on $S+\Delta-\delta$. The fields on $S+\Delta+\delta$ are then obtained from the interface condition
$$\lim_{\delta \to 0} \Psi_{S+\Delta+\delta} - \Psi_{S+\Delta-\delta} = \rho, \tag{2.8}$$
where ρ is the source on $S+\Delta$. Eqs. (2.7) and (2.8) show that if Ψ_S is known on some plane S, the transversal fields are uniquely determined everywhere in space.

6. The normal field components not included in Ψ_S are redundant and can be computed once Ψ_S is known. This will be demonstrated for Maxwell's equations in the next section.

As we shall see, these properties can be utilized to produce extremely efficient computational formulas.

3 Properties of Maxwell's equations

3.1 Diagonalization of Maxwell's equations

The derivation of the diagonalized form is given in detail in papers I (two dimensional case) and II (three dimensional case) but for the sake of completeness, we repeat the essential steps here. We start our analysis by introducing the Maxwell's curl equations in a region with no charge or current:

$$\nabla \times \vec{e} = -\mu \partial_t \vec{h}, \tag{3.1}$$
$$\nabla \times \vec{h} = \varepsilon \partial_t \vec{e}, \tag{3.2}$$

where $\vec{e}$ is the electric field and $\vec{h}$ the magnetic. Throughout this book, we will assume harmonic time dependency of the form $f(t) \sim \exp(-j\omega t)$ such that the time derivative operator ∂_t evaluates to a multiplication with $(-j\omega)$. The explicit notation of the time dependency is suppressed in all equations.

The curl operator can be written as

$$\nabla \times = \partial_x \mathbf{N}_1 + \partial_y \mathbf{N}_2 + \partial_z \mathbf{N}_3, \tag{3.3}$$

where $\mathbf{N}_i$, $i = 1, 2, 3$, are 3×3 matrices given in Eqs. (3.4)-(3.6),

$$\mathbf{N}_1 = \begin{bmatrix} 0 & 0 & 0 \\ 0 & 0 & -1 \\ 0 & 1 & 0 \end{bmatrix}, \tag{3.4}$$

$$\mathbf{N}_2 = \begin{bmatrix} 0 & 0 & 1 \\ 0 & 0 & 0 \\ -1 & 0 & 0 \end{bmatrix}, \tag{3.5}$$

$$\mathbf{N}_3 = \begin{bmatrix} 0 & -1 & 0 \\ 1 & 0 & 0 \\ 0 & 0 & 0 \end{bmatrix}. \tag{3.6}$$

Substituting Eq. (3.3) into Eqs. (3.1) and (3.2) yields

$$(\partial_x \mathbf{N}_1 + \partial_y \mathbf{N}_2 + \partial_z \mathbf{N}_3)\, \vec{e} = j\omega\mu\vec{h}, \tag{3.7}$$
$$(\partial_x \mathbf{N}_1 + \partial_y \mathbf{N}_2 + \partial_z \mathbf{N}_3)\, \vec{h} = -j\omega\varepsilon\vec{e}. \tag{3.8}$$

The z-diagonalized form can be obtained by selecting the four (out of the total six) equations where the coefficient for ∂_z are non-zero and eliminating e_z and h_z using the two remaining equations. After rearranging the terms and writing the system in a matrix form, we get the desired diagonalized equation

$$\begin{bmatrix} \mathbf{0} & \mathcal{A} \\ \mathcal{B} & \mathbf{0} \end{bmatrix} \begin{bmatrix} e_x \\ e_y \\ h_x \\ h_y \end{bmatrix} = \partial_z \begin{bmatrix} e_x \\ e_y \\ h_x \\ h_y \end{bmatrix}, \tag{3.9}$$

where $\mathbf{0}$ is a 2×2 zero matrix and the 2×2 differential operators $\mathcal{A}$ and $\mathcal{B}$ are given by

$$\mathcal{A} = \begin{bmatrix} \partial_x \frac{1}{j\omega\varepsilon} \partial_y & -\partial_x \frac{1}{j\omega\varepsilon} \partial_x + j\omega\mu \\ \partial_y \frac{1}{j\omega\varepsilon} \partial_y - j\omega\mu & -\partial_y \frac{1}{j\omega\varepsilon} \partial_x \end{bmatrix}, \tag{3.10}$$

$$\mathcal{B} = \begin{bmatrix} -\partial_x \frac{1}{j\omega\mu} \partial_y & \partial_x \frac{1}{j\omega\mu} \partial_x - j\omega\varepsilon \\ -\partial_y \frac{1}{j\omega\mu} \partial_y + j\omega\varepsilon & \partial_y \frac{1}{j\omega\mu} \partial_x \end{bmatrix}. \tag{3.11}$$

Once the transversal field is known, we can use the two remaining equations in Eq. (3.8) to solve the normal components from

$$\begin{bmatrix} e_z \\ h_z \end{bmatrix} = \mathcal{C} \begin{bmatrix} e_x \\ e_y \\ h_x \\ h_y \end{bmatrix}, \tag{3.12}$$

where the operator $\mathcal{C}$ is given by

$$\mathcal{C} = \begin{bmatrix} 0 & 0 & \frac{1}{j\omega\varepsilon} \partial_y & -\frac{1}{j\omega\varepsilon} \partial_x \\ -\frac{1}{j\omega\mu} \partial_y & \frac{1}{j\omega\mu} \partial_x & 0 & 0 \end{bmatrix}. \tag{3.13}$$

3.2 Eigenvalues and vectors

At this point, we will assume homogeneous and infinite space with no absorption or gain, i.e. ε and μ are real valued constants, and attempt to solve Eq. (3.9) in the Fourier domain. The trial function is given by

$$\Phi(\vec{r}, z) = \int \frac{d\vec{k}}{4\pi^2} \Psi(\vec{k}) \exp\left(j\vec{k} \cdot \vec{r} + \lambda z \right), \tag{3.14}$$

where the position vector $\vec{r}$ and the wave vector $\vec{k}$ are perpendicular to z-axis and $\Psi = \begin{bmatrix} e_x & e_y & h_x & h_y \end{bmatrix}^T$ is a hyper vector whose components are functions of $\vec{k}$. Substituting

Eq. (3.14) into Eq. (3.9) and equating the integrands gives

$$\begin{bmatrix} \mathbf{0} & \mathbf{A} \\ \mathbf{B} & \mathbf{0} \end{bmatrix} \begin{bmatrix} e_x \\ e_y \\ h_x \\ h_y \end{bmatrix} = \lambda \begin{bmatrix} e_x \\ e_y \\ h_x \\ h_y \end{bmatrix}, \tag{3.15}$$

where **A** and **B** are given in Eqs. (3.16) and (3.17), respectively,

$$\mathbf{A} = \begin{bmatrix} -\frac{k_x k_y}{j\omega\varepsilon} & \frac{k_x^2}{j\omega\varepsilon} + j\omega\mu \\ -\frac{k_y^2}{j\omega\varepsilon} - j\omega\mu & \frac{k_y k_x}{j\omega\varepsilon} \end{bmatrix}, \tag{3.16}$$

$$\mathbf{B} = \begin{bmatrix} \frac{k_x k_y}{j\omega\mu} & -\frac{k_x^2}{j\omega\mu} - j\omega\varepsilon \\ \frac{k_y^2}{j\omega\mu} + j\omega\varepsilon & -\frac{k_x k_y}{j\omega\mu} \end{bmatrix}. \tag{3.17}$$

Here, the parameters k_x and k_y originate from the evaluation of the spatial derivatives in the Fourier domain and are given by $k_x = \vec{k} \cdot \vec{u}_x$ and $k_y = \vec{k} \cdot \vec{u}_y$, respectively.

The eigenvectors and eigenvalues of Eq. (3.15) can be solved analytically by a straightforward calculation. There are two doubly degenerate eigenvalues

$$\lambda = \pm w = \pm\sqrt{k_x^2 + k_y^2 - \omega^2\varepsilon\mu} = \pm\sqrt{|\vec{k}|^2 - \omega^2\varepsilon\mu}, \tag{3.18}$$

and the corresponding four eigenvectors are given by

$$\Psi_\lambda^1 = \begin{bmatrix} \lambda \\ 0 \\ \frac{k_x k_y}{j\omega\mu} \\ \frac{k_y^2 - \omega^2\varepsilon\mu}{j\omega\mu} \end{bmatrix}, \; \Psi_\lambda^2 = \begin{bmatrix} 0 \\ \lambda \\ -\frac{k_x^2 - \omega^2\varepsilon\mu}{j\omega\mu} \\ -\frac{k_x k_y}{j\omega\mu} \end{bmatrix}. \tag{3.19}$$

The eigenvalue λ is a multivalued function of $\vec{k}$ with a zero crossing at $|\vec{k}| = \omega\sqrt{\varepsilon\mu}$. For $|\vec{k}| > \omega\sqrt{\varepsilon\mu}$, the eigenvalue is real, corresponding to an evanescent wave in the z-direction and for $|\vec{k}| < \omega\sqrt{\varepsilon\mu}$, the eigenvalue is imaginary, corresponding to a propagating wave. The branch of the eigenvalue should be selected based on the boundary conditions of a particular problem. The possible choices and consequent behaviours are listed in table 3.1.

The choice of the eigenvectors in Eq. (3.19) is not unique because any linear combination of eigenvectors corresponding to the same eigenvalue is also an eigenvector. In paper IV, we constructed the eigenvectors differently in order to simplify some orthogonality conditions. Furthermore, we redefined the z-dependency to be of form $f(z) \sim \exp(j\lambda z)$, which made the discussion of propagating waves simpler.

Table 3.1: The behaviour of the fields for different branches of the eigenvalue.

	$\lvert\vec{k}\rvert > \omega\sqrt{\varepsilon\mu}$	$\lvert\vec{k}\rvert < \omega\sqrt{\varepsilon\mu}$
+	$\lambda = \sqrt{\lvert\vec{k}\rvert^2 - \omega^2\varepsilon\mu}$ Evanescent wave, which decays into $z = -\infty$.	$\lambda = j\sqrt{\omega^2\varepsilon\mu - \lvert\vec{k}\rvert^2}$ Propagating wave with wave vector in the upper half plane.
-	$\lambda = -\sqrt{\lvert\vec{k}\rvert^2 - \omega^2\varepsilon\mu}$ Evanescent wave, which decays into $z = \infty$.	$\lambda = -j\sqrt{\omega^2\varepsilon\mu - \lvert\vec{k}\rvert^2}$ Propagating wave with wave vector in the lower half plane.

3.3 Solving the slab modes in terms of eigenvectors

In order to gain a qualitative understanding of the photonic crystal slab modes, we will first analyse the modes in a conventional slab waveguide.

Assume that the dielectric function is a function of z only

$$\varepsilon(z) = \begin{cases} \varepsilon_a, & z < 0 \\ \varepsilon_b, & 0 \le z < h \\ \varepsilon_c, & z \ge h \end{cases}, \tag{3.20}$$

where $\varepsilon_b > \varepsilon_a, \varepsilon_c$. Our purpose is to expand the fields in terms of the eigenvectors in each region separately and then require the continuity of the transversal field components at the interfaces. Optical modes correspond to those $[\omega, \vec{k}]$-points, for which the continuity conditions can be satisfied.

To simplify the analysis, we will make the following assumptions: *i*) The dielectric function is symmetric, i.e. $\varepsilon_a = \varepsilon_c$ and *ii*) the fields do not change in the y-direction, i.e. $\partial_y = k_y \equiv 0$. *iii*) The previous condition splits the Maxwell's equations into two independent polarisations and we will only consider the one, which has $e_x = e_z \equiv 0$. An obvious consequence is that the coefficients for the eigenvectors Ψ^1_w and Ψ^1_{-w} must be zero, because otherwise the requirement $e_x = 0$ cannot be satisfied.

For a given k_x, we can identify different ranges of ω, based on whether the eigenvectors in different regions are propagating or evanescent.

The first range is $\omega < k_x/\sqrt{\varepsilon_b\mu}$, in which the eigenvectors in all three regions are evanescent. Due to Sommerfeld's radiation condition, we have to discard all eigenvectors growing into the infinity and solutions must then be expressible in terms of four eigenvectors only: one in regions a and c and two in region b. Requiring the continuity of the transversal field components e_y and h_x on the

interfaces at $z = 0$ and $z = h$, leads to a homogeneous equation system

$$\begin{aligned} a\Psi^2_{-w_\mathrm{a}} \exp(-w_\mathrm{a} h) - b_1 \Psi^2_{-w_b} \exp(-w_\mathrm{b} h) - b_2 \Psi^2_{w_b} \exp(w_\mathrm{b} h) &= 0 \\ b_1 \Psi^2_{-w_\mathrm{b}} + b_2 \Psi^2_{w_\mathrm{b}} - c\Psi^2_{w_\mathrm{a}} &= 0 \end{aligned} \quad , \tag{3.21}$$

where the correct sign of the eigenvalue is already taken into account and hence, w_a and w_b are both assumed to be real and positive. Eq. (3.21) may have non-trivial solutions for coefficients a, b_1, b_2 and c only if the determinant of the coefficient matrix vanishes. A straightforward calculation shows that zeros of the determinant can be found at the solutions of

$$(w_\mathrm{a} - w_\mathrm{b})^2 = (w_\mathrm{a} + w_\mathrm{b})^2 \exp(2h w_\mathrm{b}) . \tag{3.22}$$

According to the assumption, both w_a and w_b are positive and real, which means that the right hand side is always larger than the left. Hence, no optical modes exist for $\omega < k_x/\sqrt{\varepsilon_\mathrm{b}\mu}$.

The second range is $k_x/\sqrt{\varepsilon_\mathrm{b}\mu} < \omega < k_x/\sqrt{\varepsilon_\mathrm{a}\mu}$, in which the eigenvectors are propagating in region b but evanescent in regions a and c. According to Sommerfeld's radiation condition, we again have to discard half of the eigenvectors in regions a and c. The zeros of Eq. (3.22) still correspond to the optical modes but now w_b is positive imaginary. It is well known that in this frequency range, Eq. (3.22) has at least one but may have more solutions and therefore we will omit the proof (see e.g. [39]). However, there is one remark we would like to make: In regions a and c, the z-component of the Poynting vector $\vec{p} = \vec{e} \times \vec{h}$ is purely imaginary, and thus, there is no energy transfer in the direction of z. Consequently, energy may propagate along the slab but not escape it, which verifies that all existing modes are bound.

The third range is $\omega > k_x/\sqrt{\varepsilon_\mathrm{a}\mu}$, in which the eigenvectors are propagating in all three regions. Now we can adopt one of the following interpretations: *i*) None of the eigenvectors in regions a or c decay in infinity and therefore, we discard them all. *ii*) None of the eigenvectors in regions a or c explode in infinity either and therefore we include them all. In the first case, it can be easily shown that the interface conditions cannot be satisfied with only the two remaining eigenvectors in region b and consequently, there can be no modes. The second choice leads to a total of six usable eigenvectors but only four equations emerging from the interface conditions. Hence, solutions may be found for any $[\omega, \vec{k}]$-point if two of the coefficients are fixed arbitrarily.

We summarize these results in terms of an example. Assume for a moment that Ξ in

$$\Xi \vec{h} = \omega^2 \vec{h} \tag{3.23}$$

is the Helmholtz operator for the particular geometry described in Eq. (3.20) and $\vec{h}$ denotes the magnetic field in all space (that is, in regions a, b and c). Then, the spectrum of the eigenvalues of Ξ *i*) vanishes for $\omega < |\vec{k}|/\sqrt{\varepsilon_\mathrm{b}\mu}$, *ii*) is discrete for $|\vec{k}|/\sqrt{\varepsilon_\mathrm{b}\mu} < \omega < |\vec{k}|/\sqrt{\varepsilon_\mathrm{a}\mu}$ where bound modes can exist and *iii*) is continuous for $\omega > |\vec{k}|/\sqrt{\varepsilon_\mathrm{a}\mu}$, where the modes are not bound to the slab. The relation

$$\omega_\mathrm{ll} = \frac{|\vec{k}|}{\sqrt{\max(\varepsilon_\mathrm{a}, \varepsilon_\mathrm{c})\mu}} \tag{3.24}$$

is called a light line. All modes with $\omega < \omega_\mathrm{ll}$ have to be bound as there are no propagating states in the cladding.

4 Algorithm for photonic crystal slabs

Our aim is to develop a computational formula for the generalized photonic crystal slab defined in Eq. (2.1). We will assume all dielectrics to be isotropic and linear but generally frequency dependent and complex valued. For practical reasons, magnetic permeability μ is assumed to be constant but this requirement can be relaxed easily.

Our strategy is to expand the x- and y-dependency of the fields using planewaves. The z-dependency of the fields will be expanded in terms of finite differences inside the slab and in terms of homogeneous-medium eigenvectors in the claddings. Finally, a system matrix is created by requiring the continuity of the tangential fields on the interfaces between the slab and the claddings.

4.1 Planewave expansion

Our starting point is the planewave expansion in two dimensions

$$\Psi(\vec{r},z) = \sum_n \Psi_n(z) \exp\left[j(\vec{g}_n + \vec{k}) \cdot \vec{r} \right], \tag{4.1}$$

where Ψ_n is a hypervector whose elements are still unspecified $z-$dependent coefficients for the transversal field components e_x, e_y, h_x and h_y and the summation extends over some truncated set of the reciprocal lattice vectors $\vec{g}_n$. The coefficient $\vec{k}$ deserves a little bit more attention: According to Floquet's theorem, a differential equation with a periodic potential has a solution of a form

$$f(\vec{r}) = \exp(j\vec{k}\cdot\vec{r})u(\vec{r}), \tag{4.2}$$

where $u(\vec{r})$ shares periodicity with the lattice and $\exp(j\vec{k}\cdot\vec{r})$ is a phase factor. Therefore, $\vec{k}$ specifies the phase change as the wave propagates from one unit cell to next or equivalently, imposes the Bloch periodic boundary condition.

4.2 Finite difference discretization

Inside the slab, we discretize the fields on a finite number of planes defined by $z = z^{(i)} = i\Delta$, where Δ is the finite difference step length. The electric fields at planes $z^{(i+0.5)} = (i+0.5)\Delta$ and $z^{(i-0.5)} = (i-0.5)\Delta$ can be related to each other using a first order finite difference scheme

$$\partial_z e(z)|_{z=z^{(i)}} = \frac{e^{(i+0.5)} - e^{(i-0.5)}}{\Delta}, \tag{4.3}$$

where either e_x or e_y may be substituted in place of e. Adopting a notation $\vec{e} = \begin{bmatrix} e_x & e_y \end{bmatrix}^T$, we can write a vector identity

$$\vec{e}^{(i+0.5)} = \vec{e}^{(i-0.5)} + \Delta \left(\partial_z \vec{e}\right)^{(i)}. \tag{4.4}$$

Given the knowledge of $\vec{h}^{(i)} = \begin{bmatrix} h_x^{(i)} & h_y^{(i)} \end{bmatrix}^T$, the required derivative can be computed from

$$\left(\partial_z \vec{e}\right)^{(i)} = \mathcal{A}^{(i)} \vec{h}^{(i)}, \tag{4.5}$$

where $\mathcal{A}$ is defined in Eq. (3.10) and the superscript (i) indicates that the material parameters should be evaluated at $z = i\Delta$.

In order to turn Eq. (4.4) into a useful numerical formula, we need to introduce the field expansion given in Eq. (4.1) and create a discrete representation of $\mathcal{A}$. Since this derivation is rather lengthy and will be substituted with a more efficient procedure in the final algorithm to be discussed in chapter 6, we will only describe the steps qualitatively. The complete derivation, albeit only in the 2D case, is given in publication I.

1. Divide Eq. (4.4) into separate equations for e_x and e_y and focus on e_x.

2. Substitute the planewave expansion for e_x, h_x and h_y.

3. Multiply both sides with $\exp[-j(\vec{g}_m + \vec{k}) \cdot \vec{r}]$ for each $m \in [0, N-1]$, where N is the number of planewaves in the truncated basis. This gives N equations for the N expansion coefficients.

4. Evaluate the positional derivatives and integrate both sides over one unit cell of the lattice in order to eliminate the $\vec{r}$-dependency. On the right hand side, one needs to use the differentiation rule for products and partial integration so that the spatial function ε does not have to be differentiated explicitly. Integrals not involving ε can be evaluated using the orthogonality of the planewaves. The rest of the integrals can be evaluated numerically using the Fast Fourier Transform (FFT).

5. Perform similar steps on the other equation for e_y.

The result of this procedure is a linear equation system for the planewave coefficients of the fields. The discrete version of $\mathcal{A}$ is a $2N \times 2N$ matrix, whose elements depend in a complicated way on the dielectric function evaluated at $z = i\Delta$ and Fourier space representations of the spatial derivatives.

Performing similar manipulations on the equation where $\vec{e}$ and $\vec{h}$ are interchanged, we get two matrix equations

$$\mathbf{e}^{(i+0.5)} = \mathbf{e}^{(i-0.5)} + \Delta \mathbf{A}^{(i)} \mathbf{h}^{(i)}, \tag{4.6}$$

$$\mathbf{h}^{(i+1)} = \mathbf{h}^{(i)} + \Delta \mathbf{B}^{(i+0.5)} \mathbf{e}^{(i+0.5)}, \tag{4.7}$$

where $\mathbf{A}$ and $\mathbf{B}$ are the discrete versions of $\mathcal{A}$ and $\mathcal{B}$, respectively and

$$\mathbf{h}^{(i)} = \begin{bmatrix} h_{x,0}^{(i)} & . & . & . & h_{x,N-1}^{(i)} & h_{y,0}^{(i)} & . & . & . & h_{y,N-1}^{(i)} \end{bmatrix}^T, \tag{4.8}$$

contains the planewave coefficients for the magnetic field defined at $z = i\Delta$ and similarly for the other vectors involved.

Eqs. (4.6) and (4.7) form a coupled system. Once the $\mathbf{h}^{(i)}$ and $\mathbf{e}^{(i-0.5)}$ are known for some value of i, they can be computed for any value of i. Obviously, we need to start somewhere and therefore we will next turn our attention to the boundary conditions in the claddings.

4.3 Eigenvector expansion in the claddings

We will expand the fields in the claddings in terms of the eigenvectors of the diagonalized form given in Eq. (3.9). We first consider claddings where the dielectric function shares periodicity with the slab and then give an analytic formula for the eigenvectors in the special case of homogeneous claddings.

Because the dielectric function is periodic, the eigenvectors can once again be expanded in terms of planewaves

$$\Psi(\vec{r},z) = \sum_n \Psi_n \exp\left[j(\vec{g}_n + \vec{k})\cdot\vec{r} + \lambda z\right], \tag{4.9}$$

where Ψ_n is a coefficient for the transversal fields and the exponential z-dependency is introduced because the eigenvalue we are looking for is the propagation constant in the z-direction. The eigenvectors can be computed numerically as follows: *i*) substitute the planewave expansion of Eq. (4.9) into the diagonalized form, *ii*) create discrete representations of all the differential operators along the guidelines given in the preceding section and *iii*) solve the resulting algebraic eigenvalue equation for the $4N$ eigenvalues and eigenvectors.

The general expression of the fields is then given by

$$\Psi(\vec{r},z) = \sum_{l=0}^{4N-1} \gamma_l \exp(\lambda_l z) \sum_{n=0}^{N-1} \Psi_{l,n} \exp\left[j(\vec{g}_n + \vec{k})\cdot\vec{r}\right], \tag{4.10}$$

where $\Psi_{l,n}$ is the nth coefficient for the lth eigenvector, λ_l is the corresponding eigenvalue and γ_l is a scalar weight factor.

The general expression can be greatly simplified if the material parameters ε and μ do not vary in space. To see why this happens, substitute the planewave expansion given in Eq. (4.9) into the diagonalized form in order to get

$$\mathcal{L}\sum_n \Psi_n \exp\left[j(\vec{g}_n + \vec{k})\cdot\vec{r}\right] = \lambda \sum_n \Psi_n \exp\left[j(\vec{g}_n + \vec{k})\cdot\vec{r}\right]. \tag{4.11}$$

Evaluate the positional derivatives in $\mathcal{L}$ using the property that all the parameters are position independent and therefore commute with the derivatives. This gives

$$\sum_n \mathbf{L}_n \Psi_n \exp\left[j(\vec{g}_n + \vec{k})\cdot\vec{r}\right] = \lambda \sum_n \Psi_n \exp\left[j(\vec{g}_n + \vec{k})\cdot\vec{r}\right], \tag{4.12}$$

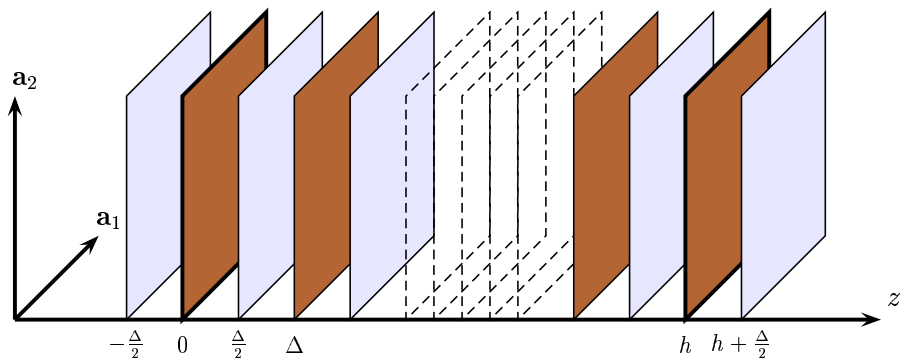

Figure 4.1: The discretization scheme. The planewave expansion of the electric field on light coloured planes is related to the planewave expansion of the magnetic field on the dark coloured planes using finite differences. The eigenvector expansions for $z < 0$ and $z > h$ act as boundary conditions and are used for terminating the finite difference grid.

where $\mathbf{L}_n$ is a 4×4 matrix. Multiply both sides with $\exp[-j(\vec{g}_m + \vec{k}) \cdot \vec{r}]$ for each $m \in [0, N-1]$, integrate over the unit cell and use the orthogonality of the harmonic functions to get

$$\mathbf{L}_n \Psi_n = \lambda \Psi_n. \tag{4.13}$$

The orthogonality of the basis set thus decoupled the general $4N \times 4N$ algebraic eigenvalue equation into N independent 4×4 eigenvalue equations. Furthermore, each of these N equations is equivalent with the eigenvalue equation given in Eq. (3.15), which we have already solved. The implication on Eq. (4.10) is that the summation over l extends now only over the four eigenvectors for each planewave n. Further simplifications are possible by noting that eigenvectors growing into infinity do not satisfy the Sommerfeld's radiation condition and should be discarded. This leaves us with an expansion of a form

$$\Psi(\vec{r}, z) = \sum_{n=0}^{N-1} \exp\left[j(\vec{g}_n + \vec{k}) \cdot \vec{r} + \lambda_n z \right] \left(\alpha_n \Psi_n^1 + \beta_n \Psi_n^2 \right), \tag{4.14}$$

where Ψ_n^1 and Ψ_n^2 are the eigenvectors given in Eq. (3.19), corresponding to the planar wave vector $(\vec{g}_n + \vec{k})$ and α_n and β_n are their scalar weight coefficients. The sign of the eigenvalue λ_n should be chosen according to the discussion in section 3.2. The discretization scheme is illustrated in Fig. 4.1.

The eigenvector expansion given in Eq. (4.10) can also be used for describing the fields in the slab, provided that the slab is homogeneous in z or can be divided into thinner slabs which are. The advantage over the finite difference scheme is that the z-dependency for each eigenvector is analytically known and we can, in principle, expand the fields in the whole slab using only the $4N$ eigenvectors. This appears to give tremendous savings compared to the finite difference scheme where we need $4N$ variables for each thin layer of thickness Δ. Unfortunately, eigenvector expansion is not as efficient as it seems because all the $4N$ eigenvectors have to be computed

numerically. Since N typically varies between 200 and 2000, this is a daunting task for today's computers.

Expanding the fields in terms of the eigenvectors both in the slab and in the claddings is actually a variant of the transfer matrix method. In the course of this work, we essayed this in 2D and 3D coordinates. The 2D version gave reasonable results but the 3D version was orders of magnitude slower than the finite difference scheme and was therefore soon discarded. Furthermore, the transfer matrix method is not numerically stable since both the decaying and increasing eigenvectors are included, which causes round-off errors in thick slabs [32].

4.4 Matching the interface conditions

The finite difference grid provides us with the value of the electric field at $z = -0.5\Delta$ and magnetic field at $z = 0$. The grid can be terminated to an open boundary condition by relating these two together using the homogeneous-medium eigenvectors. Four sets of boundary conditions are needed but we will only discuss one of them at $z = 0$ as the other three can be derived in a very similar fashion. The treatment is simplified by the decoupling property of the planewaves in a homogeneous medium, which allows us to treat each planewave $(\vec{g}_n + \vec{k})$ independently.

For a given n, the field coefficients in the lower cladding ($z < 0$) are given by

$$\Psi_n^-(z) = \left(\alpha_n \Psi_n^{1-} + \beta_n \Psi_n^{2-}\right) \exp\left(\lambda_n^- z\right), \tag{4.15}$$

where the minus sign is used to indicate the lower half space. For brevity, we will omit the minus sign and the index n from the notation in the following discussion. Particularly, we have

$$h_x(z) = \left(\alpha \Psi^1[3] + \beta \Psi^2[3]\right) \exp\left(\lambda z\right), \tag{4.16}$$

where the number three in the square brackets denotes the third component of the eigenvector. A careful inspection of the definition of the eigenvectors in Eq. (3.19) reveals that $e_x(0) = \lambda\alpha$ and $e_y(0) = \lambda\beta$ and therefore we can write

$$\lambda h_x(0) = e_x(0)\Psi^1[3] + e_y(0)\Psi^2[3]. \tag{4.17}$$

This is almost the desired boundary condition equation, except that the finite difference discretization gives us electric fields at $z = (i + 0.5)\Delta$ for integer values of i. This problem is solved by noting that we know the functional form of z-dependency and therefore obtain

$$\lambda h_x(0) = \left(e_x(-0.5\Delta)\Psi^1[3] + e_y(-0.5\Delta)\Psi^2[3]\right) \exp\left(0.5\Delta\lambda\right). \tag{4.18}$$

Finally, adopting the notation of discrete fields and reintroducing the planewave index n, we get

$$\left(e_{x,n}^{(-0.5)}\Psi_n^{1-}[3] + e_{y,n}^{(-0.5)}\Psi_n^{2-}[3]\right) \exp\left(0.5\Delta\lambda_n^-\right) - \lambda_n^- h_{x,n}^{(0)} = 0. \tag{4.19}$$

Proceeding in a similar fashion, the remaining three boundary conditions can be constructed.

4.5 Putting it all together

In the previous sections we developed a method for relating the electric and magnetic field coefficients to each other in the slab using a finite difference grid and boundary conditions for terminating the grid at the interfaces of the slab. The whole problem can now be collected into one equation by discretizing operators $\mathcal{A}$ and $\mathcal{B}$ on each discrete plane $z^{(i)}$ within the slab and computing the eigenvectors and eigenvalues in the claddings. This leads to a homogeneous equation system

$$\mathbf{M}(\omega, \vec{k}, \varepsilon, \mu)\mathbf{f} = \mathbf{0}, \tag{4.20}$$

where $\mathbf{M}$ contains all the discrete operators and boundary conditions and $\mathbf{f}$ contains all the field coefficients. There are $2(2I+1)N$ unknowns, since the two components of the magnetic fields are discretized on I planes and electric field components on $(I+1)$ planes and each of the field components is expanded in terms of N planewaves. Eigenmodes of the photonic crystal slab correspond to those $[\omega, \vec{k}]$-pairs, for which Eq. (4.20) has non-trivial solutions, or equivalently, $\mathbf{M}(\omega, \vec{k})$ is singular.

We also investigated an alternative way of formulating the eigenproblem, which is theoretically appealing but was found to be numerically unstable and inefficient. The algorithm is briefly explained below:

1. Take the planewave coefficients of the electric field in the lower cladding, $\mathbf{e}^{(-0.5)}$, to be the unknown vector.

2. Compute the planewave coefficients of the magnetic field in the lower cladding from $\mathbf{h}^{(0)} = \mathbf{C}_l \mathbf{e}^{(-0.5)}$, where $\mathbf{C}_l$ is a matrix constructed from the homogeneous-medium eigenvectors as described in section 4.4.

3. Compute electric and magnetic fields recursively from $\mathbf{e}^{(i+0.5)} = \mathbf{e}^{(i-0.5)} + \Delta\mathbf{A}^{(i)}\mathbf{h}^{(i)}$ and $\mathbf{h}^{(i+1)} = \mathbf{h}^{(i)} + \Delta\mathbf{B}^{(i)}\mathbf{e}^{(i+0.5)}$, respectively, until one ends up with two equations $\mathbf{e}^{(I+0.5)} = \mathbf{G}_e\mathbf{e}^{(-0.5)}$ and $\mathbf{h}^{(I)} = \mathbf{G}_h\mathbf{e}^{(-0.5)}$, where $h = z_I = I\Delta$ is the thickness of the slab and $\mathbf{G}_e$ and $\mathbf{G}_h$ are $2N \times 2N$ matrices.

4. Use the eigenvectors in the upper cladding to get $\tilde{\mathbf{e}}^{(I+0.5)} = \mathbf{C}_u\mathbf{h}^{(I)}$. Equate the two candidates for the electric field at $z = (I+0.5)\Delta$ to get

$$\tilde{\mathbf{M}}\mathbf{e}^{(-0.5)} = (\mathbf{G}_e - \mathbf{C}_u\mathbf{G}_h)\mathbf{e}^{(-0.5)} = 0. \tag{4.21}$$

The eigenmodes of the slab system are again found at the singular points of $\tilde{\mathbf{M}}$, which now has a dimension of only $2N \times 2N$. Even though the resulting system matrix is very small compared to the system matrix in Eq. (4.20), there are a number of undesired properties: *i*) The construction of $\tilde{\mathbf{M}}$ is very tedious as it requires many multiplications between full matrices of size $2N \times 2N$. *ii*) $\tilde{\mathbf{M}}$ is a full matrix and Eq. (4.21) is nearly impossible to solve using iterative solvers. Therefore, the efficient operator level techniques to be discussed in section 6 cannot used. *iii*) Finally, the process of constructing $\tilde{\mathbf{M}}$ is not numerically stable, which was also observed by Pendry *et al.* [30]. The instability is related to the presence of the exponentially growing and decaying eigenvectors within the slab, even though they are not explicitly considered in the finite difference formalism.

5 Algorithm for cylindrical coordinates

In this section, we consider problems which are periodic only along the z-axis and non-periodic on the transversal plane. Our strategy is to use cylindrical coordinates and diagonalize Maxwell's equations along the radial direction. The introduction of cylindrical coordinates automatically makes the geometry periodic along the angular direction ϕ and hence, we can expand the transversal fields on discrete cylindrical surfaces $r^{(i)} = i\Delta$ in terms of planewaves[1]. The planewave expansions on adjacent cylindrical surfaces are again related through finite differences. Examples of problems where this approach is suitable include a Bragg fiber and especially, a Bragg fiber which does not possess a complete cylindrical symmetry.

We start by introducing the curl operator in cylindrical coordinates

$$\nabla \times \vec{f} = \frac{1}{r} \begin{vmatrix} \vec{u}_r & r\vec{u}_\phi & \vec{u}_z \\ \partial_r & \partial_\phi & \partial_z \\ f_r & r f_\phi & r_z \end{vmatrix}, \tag{5.1}$$

where $\vec{u}_r$, $\vec{u}_\phi$ and $\vec{u}_z$ are the unit vectors in radial, angular and z-direction, respectively. Substituting Eq. (5.1) into Maxwell's curl equations and proceeding along the guidelines depicted in section 3.1, results in an equation of the following form:

$$\mathcal{L}(\partial_z, \partial_\phi, \varepsilon, \mu) \begin{bmatrix} e_z \\ re_\phi \\ h_z \\ rh_\phi \end{bmatrix} = \partial_r \begin{bmatrix} e_z \\ re_\phi \\ h_z \\ rh_\phi \end{bmatrix}. \tag{5.2}$$

This is not the radially diagonalized form yet because the r-dependency is still explicit. However, a simple variable substitution $r f_\phi \rightarrow \widehat{f}_\phi$ for both e_ϕ and h_ϕ is sufficient to bring Eq. (5.2) into the proper diagonalized form.

The field expansion is similar to the Cartesian coordinate system: for a constant $r^{(i)} = i\Delta$, the fields are expressed as

$$\Psi^{(i)}(\phi, z) = \sum_{m,n} \Psi^{(i)}_{m,n} \exp\left[j2\pi m\phi + j\left(\frac{2\pi n}{L_z} + k\right) z \right], \tag{5.3}$$

where $\Psi = \begin{bmatrix} e_z & \widehat{e}_\phi & h_z & \widehat{h}_\phi \end{bmatrix}^T$ is a hypervector of the transversal field components and k implements the Bloch periodic boundary condition in the z-direction. There is no Bloch term in the angular direction as a translation over the periodicity interval 2π returns to the same point

[1] Completely non-periodic problems could be solved using a similar procedure in spherical coordinates but this remains a topic of future research.

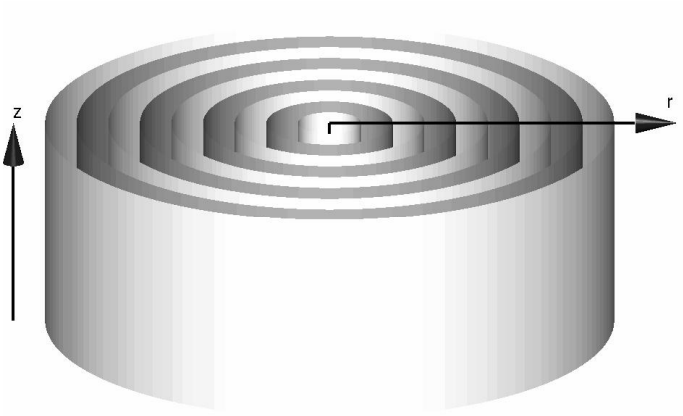

Figure 5.1: The discretization scheme in cylindrical coordinates. Electric field is expanded in terms of planewaves on the light coloured cylindrical surfaces and magnetic on the dark. The fields on adjacent surfaces are related through finite differences and outside the outermost surface, the fields are expanded in terms of eigenvectors. The geometry is assumed to be periodic in the z-direction.

and hence, the fields cannot experience a phase shift. Please note that problems which are homogeneous in z, such as optical fibers, can be solved by expanding the fields using only a single planewave in the z-direction [40].

The implementation of finite differences is as before: The radial derivative of the electric fields is completely determined by the magnetic fields and vice versa and the fields can be discretized in an interlaced grid as illustrated in Fig. 5.1.

5.1 Boundary conditions in cylindrical coordinates

The boundary conditions in cylindrical coordinates are more complicated than in Cartesian but the basic principles still apply: We need four sets of boundary conditions in order to terminate the finite difference grid.

The outer boundary is similar to the Cartesian slab boundary: we can analytically solve the four eigenvectors and eigenvalues of Eq. (5.2), select the two which decay for $r \to \infty$ and relate the electric and magnetic fields to each other in a way discussed in section 4.3. The eigenfunctions in cylindrical coordinates, which are given in publication III, are composed of Hankel functions and their derivatives.

The remaining two boundary conditions are applied around the center axis of the cylinder, i.e. in the vicinity of $r = 0$. The first one them is very simple. We set $\widehat{h}_\phi = 0$ at $r = 0$, which is possible because any vector with one endpoint in the origin is a position vector and can be expressed in terms of $\vec{u}_r$ only. This claim is actually already implied in the variable substitution $\widehat{h}_\phi = r h_\phi$,

because if $\widehat{h}_\phi$ did not vanish in the origin, h_ϕ would obtain infinite values which is clearly not physical.

It would be tempting to use similar reasoning for $\widehat{e}_\phi$ as well. However, in the finite difference grid, electric fields are defined at $r = (i + 0.5)\Delta$, which means that the coefficients $\widehat{\mathbf{e}}_\phi^{(0)}$ are not easily available. Therefore we use Faraday's law in integral form, given in Eq. (5.4), for relating the coefficient vectors $\widehat{\mathbf{e}}_\phi^{(0.5)}$ and $\mathbf{h}_z^{(0)}$ to each other,

$$\oint_L \vec{e} \cdot d\vec{l} = \int_S j\omega\mu\vec{h} \cdot d\vec{S}. \tag{5.4}$$

Here, L is a closed path which we choose to coincide with $r = 0.5\Delta$ such that the scalar product can be easily evaluated using the coefficients $\widehat{\mathbf{e}}_\phi^{(0.5)}$. An approximation to the surface integral over S on the right hand side can be computed using the coefficients $\mathbf{h}_z^{(0)}$, which are also present in the finite difference grid. Equations for individual coefficients can be obtained by substituting the relevant field expansions into Eq. (5.4), performing the integrals and then applying the orthogonality of the basis functions.

6 Solving the equation system

Whether we are working in 2D or 3D Cartesian coordinates or cylindrical coordinates, collecting all the finite difference equations and boundary conditions into one matrix and all the field expansion coefficients into one vector, results in an equation system of the form given in Eq. (4.20). To make the discussion more explicit, we write Eq. (4.20) out in more detail for the 3D Cartesian coordinate system

$$\begin{bmatrix} \mathbf{C}_1^l & \mathbf{C}_2^l & & & & & & & \\ \mathbf{I} & \Delta\mathbf{B}^{(0)} & -\mathbf{I} & & & & & & \\ & \mathbf{I} & \Delta\mathbf{A}^{(0.5)} & -\mathbf{I} & & & & & \\ & & \cdot & \cdot & \cdot & & & & \\ & & & \cdot & \cdot & \cdot & & & \\ & & & & \cdot & \cdot & \cdot & & \\ & & & & & \mathbf{I} & \Delta\mathbf{B}^{(I)} & -\mathbf{I} & \\ & & & & & & \mathbf{C}_1^u & \mathbf{C}_2^u & \end{bmatrix} \begin{bmatrix} \mathbf{e}^{(-0.5)} \\ \mathbf{h}^{(0)} \\ \mathbf{e}^{(0.5)} \\ \cdot \\ \cdot \\ \cdot \\ \mathbf{h}^{(I)} \\ \mathbf{e}^{(I+0.5)} \end{bmatrix} = \mathbf{0}. \tag{6.1}$$

Here, $\mathbf{A}^{(i)}$ and $\mathbf{B}^{(i)}$ are the discrete representations of $\mathcal{A}$ and $\mathcal{B}$ on a plane $z = i\Delta$. Submatrices $\mathbf{C}_m^u$ ($\mathbf{C}_m^l$), where the superindex u (l) denotes the upper (lower) boundary of the slab, implement the boundary conditions as discussed in section section 4.3.

Non-trivial solutions to the system equation may exist only if the system matrix $\mathbf{M}$ is singular or equivalently, its determinant vanishes. There are a number of methods for testing matrix singularity and we will discuss some approaches tried in this work.

6.1 Solving the bands

Whatever the measure of singularity we use, our strategy for finding the bands is to fix the Bloch vector $\vec{k}$ and then vary ω until a singular point of $\mathbf{M}$ is found. Obviously, the efficiency of the searching algorithm is very important because computing the measure of singularity is always tedious for big matrices. Our preferred strategy is to step ω at an adaptive interval until a singular point is bracketed and then switch to the Golden section search [41] in order to iterate the point sharply. This approach was used with little modifications for all geometries and coordinate systems. Paper I discusses the issue in more depth.

The most straightforward way of estimating matrix singularity, computing its determinant, is often criticized because determinants lack an absolute scale. This means that a nearly singular matrix may have a very big determinant (and vice versa) and the singularity cannot be detected if the

determinant is not exactly zero, which is rarely the case in numerical computation. In our application, however, the determinant can be successfully used since we search for local minima by varying a parameter such that the absolute value is insignificant. The bands of a 2D slab were computed using the determinant and the performance was found to be satisfactory [37]. In order to avoid numerical overflow, we performed a *LU*-decomposition on the system matrix and added the logarithms of the diagonal elements instead of multiplying them together.

Another measure for singularity of a matrix is its 2-norm condition number (or its inverse), i.e. the ratio of its largest and smallest singular values. This approach was also tested on the 2D Cartesian system but the accuracy was not very good because the objective function $f_{\tilde{k}}(\omega) = 1/\mathrm{cond}(\mathbf{M}_{\tilde{k}}(\omega))$ was noisy and its minima were difficult to distinguish. This was the case, at least, when the singular values were solved using standard computational tools, such as the Lapack-library [42]. The explanation for this behaviour was not explored further because computing singular values is computationally more expensive than computing determinants anyway.

Yet another measure for singularity is the magnitude of the smallest eigenvalue of a matrix. This can be justified as follows: Assume for a moment that $\mathbf{M}$ has an eigenvalue zero. Then, the system $\mathbf{Mf} = \lambda\mathbf{f}$ has a solution for $\lambda = 0$. Obviously, the eigenvector corresponding to the eigenvalue $\lambda = 0$ is also a solution to the homogeneous equation $\mathbf{Mf} = \mathbf{0}$. This approach was discarded for same reasons as the singular value decomposition: it was noisy and computationally expensive.

For 3D Cartesian and cylindrical coordinates, $\mathbf{M}$ becomes very large and a direct factorization of any kind is often too expensive. Therefore, we developed a scheme for determining the matrix singularity from the solution of an ordinary equation

$$\mathbf{Mf} = \mathbf{s}, \tag{6.2}$$

where $\mathbf{s}$ is some force term. In the following sections we will discuss how to give $\mathbf{s}$ a physically meaningful content but first we concentrate on finding the eigenmodes of the slab problem, i.e. the singular points of $\mathbf{M}$, based on the properties of $\mathbf{f}$.

Assume that *i*) $\mathbf{M}$ approaches singularity and therefore has an eigenvalue close to 0 and *ii*) $\mathbf{s}$ is an excitation with suitable properties to be defined below. Then, it can be shown that the solution $\mathbf{f}$ approaches to an eigenvector of $\mathbf{M}$, corresponding to the eigenvalue 0. Furthermore, the Euclidean norm $||\mathbf{f}||_2$ approaches infinity. The formal proof to this theorem is given in paper II and some related information in Ref. [43].

The practical value of the above theorem is that using the value $||\mathbf{f}||_2$ (or inverse) as a measure of singularity, we can avoid the direct factorization of $\mathbf{M}$ and solve Eq. (6.2) using efficient iterative techniques to be discussed in section 7. Almost any choice of $\mathbf{s}$ will do. Only if $\mathbf{s}$ is algebraically orthogonal to the eigenvector corresponding to the eigenvalue 0, the above theorem fails.

6.2 Current excitations

One of the great features of the diagonalized form is that only the transversal field components enter the formulation, which makes it particularly easy to implement various kinds of interface

conditions. In this section, we will show how to incorporate surface currents into the discrete system equation given in Eq. (6.2).

In the presence of a surface current, the transversal magnetic field experiences a jump discontinuity given by

$$\vec{u}_\perp \times (\vec{h}_{||}^{+} - \vec{h}_{||}^{-}) = \vec{j}_{||}, \tag{6.3}$$

where $\vec{h}_{||}^{+}$ ($\vec{h}_{||}^{-}$) is the transversal magnetic field immediately above (below) the surface, $\vec{u}_\perp$ is a unit vector in the direction of surface normal and $\vec{j}_{||}$ is the surface current per unit length. Since $\vec{u}_\perp$ has a length of unity and $\vec{u}_\perp$ and $\vec{h}_{||}$ are orthogonal by definition, Eq. (6.3) can be inverted to read

$$\vec{h}_{||}^{+} - \vec{h}_{||}^{-} = -\vec{u}_\perp \times \vec{j}_{||}. \tag{6.4}$$

Next, consider the transversal magnetic field on two closely spaced surfaces $z = z_0 + \delta$ and $z = z_0 - \delta$, and expand the fields in two Taylor series:

$$\vec{h}_{||}\left(z_0 + \delta + \frac{\Delta}{2}\right) = \sum_{n=0}^{\infty} \frac{1}{n!}\left(\frac{\Delta}{2}\right)^n \left(\partial_z^n \vec{h}_{||}(z)\right)\Big|_{z=z_0+\delta}, \tag{6.5}$$

$$\vec{h}_{||}\left(z_0 - \delta - \frac{\Delta}{2}\right) = \sum_{n=0}^{\infty} \frac{1}{n!}\left(-\frac{\Delta}{2}\right)^n \left(\partial_z^n \vec{h}_{||}(z)\right)\Big|_{z=z_0-\delta}. \tag{6.6}$$

Keeping only the terms up to $n = 1$ and subtracting Eq. (6.6) from Eq. (6.5) yields

$$\vec{h}_{||}\left(z_0 + \delta + \frac{\Delta}{2}\right) - \vec{h}_{||}\left(z_0 - \delta - \frac{\Delta}{2}\right) =$$

$$\vec{h}_{||}(z_0 + \delta) - \vec{h}_{||}(z_0 - \delta) + \frac{\Delta}{2}\vec{h}'_{||}(z_0 + \delta) + \frac{\Delta}{2}\vec{h}'_{||}(z_0 - \delta), \tag{6.7}$$

where the prime denotes a derivative with respect to z. Letting $\delta \to 0$ and using Eq. (6.4), gives

$$\vec{h}_{||}\left(z_0 + \frac{\Delta}{2}\right) - \vec{h}_{||}\left(z_0 - \frac{\Delta}{2}\right) = -\vec{u}_S \times \vec{j}_{||} + \Delta\vec{h}'_{||}(z_0). \tag{6.8}$$

Introducing the planewave expansion and rewriting this equation in the notation used in Eq. (6.1), gives

$$\mathbf{h}^{(i)} + \Delta\mathbf{B}^{(i+0.5)}\mathbf{e}^{(i+0.5)} - \mathbf{h}^{(i+1)} = \mathbf{j}^{(i+0.5)}, \tag{6.9}$$

where $\mathbf{j}^{(i+0.5)} = \begin{bmatrix} -\mathbf{j}_y^{(i+0.5)} & \mathbf{j}_x^{(i+0.5)} \end{bmatrix}^T$ is a vector composed of the planewave coefficients for the y- and x- components of the surface current on the plane $z = (i + 0.5)\Delta$.

This result confirms that current excitations yield no modification on the system matrix in Eq. (6.1), as the only difference is the force term on the right hand side. Obviously, a similar procedure is equally applicable to 2D Cartesian and cylindrical coordinates. It should be noted, though, that expanding the surface current in the planewave basis implies the Bloch periodic boundary condition automatically. This means that the surface current term $\vec{j}$ actually implements a phased array of currents.

6.3 Scattering problems

We next turn our attention to computing the fields in the presence of an incident field. We will express the incident field in terms of the homogeneous-medium eigenvectors and then incorporate them to the boundary condition equations. As an example, we will show how to do this for a wave propagating from $z = -\infty$ towards the slab boundary at $z = 0$.

The homogeneity of the medium and the orthogonality of the harmonic basis allow us to consider each planewave coefficient independently. Hence, for a given planewave with the planar wave vector $(\vec{g}_n + \vec{k})$ the incident field can be written as

$$\Psi_n^+(z) = \left(\alpha_n \Psi_n^{1+} + \beta_n \Psi_n^{2+}\right) \exp\left(\lambda_n^+ z\right), \tag{6.10}$$

where the eigenvectors Ψ_n^1 and Ψ_n^2 are defined in Eq. (3.19) and α_n and β_n are scalar weight coefficients. The superindex "+" indicates that the eigenvalue λ should be chosen such that energy flows towards the slab.

Next we focus on the boundary condition Eq. (4.19), which is reviewed here for convenience,

$$\left[e_{x,n}^{(-0.5)} \Psi_n^{1-}[3] + e_{y,n}^{(-0.5)} \Psi_n^{2-}[3]\right] \exp\left(0.5\Delta\lambda_n^-\right) - \lambda_n^- h_{x,n}^{(0)-} = 0. \tag{6.11}$$

Observe carefully that the variable $h_{x,n}^{(0)-}$ represents the x-directional component of the magnetic field of the outgoing eigenvectors. However, in the system equation given in Eq. (6.1), $h_{x,n}^{(0)}$ is taken to be the total x-component of the magnetic field. In the absence of the incident field, these are naturally the same thing. Since we now assume an incident field to be present, we must distinguish between the two and write $h_{x,n}^{(0)} = h_{x,n}^{(0)-} + h_{x,n}^{(0)+}$. Solving for $h_{x,n}^{(0)-}$ and substituting into Eq. (6.11) gives

$$\left[e_{x,n}^{(-0.5)} \Psi_n^{1-}[3] + e_{y,n}^{(-0.5)} \Psi_n^{2-}[3]\right] \exp\left(0.5\Delta\lambda_n\right) - \lambda_n^- h_{x,n}^{(0)} = -\lambda_n^- h_{x,n}^{(0)+}. \tag{6.12}$$

The form in Eq. (6.12) differs from Eq. (6.11) only in its right hand side and can therefore be directly substituted into the system equation. Obviously, a similar treatment can be given to the other boundary condition equation concerning h_y.

We still need to tie the electric field part of the incident field to the system equation. Consider the second row of Eq. (6.1), which reads

$$\mathbf{e}^{(-0.5)} + \Delta\mathbf{B}^{(0)}\mathbf{h}^{(0)} - \mathbf{e}^{(0.5)} = \mathbf{0}. \tag{6.13}$$

The situation is now opposite to the previous boundary condition we just derived: $\mathbf{e}^{(-0.5)}$ in Eq. (6.13) should represent the total electric field on plane $z = -0.5\Delta$ but only the outgoing part is present in the system equation in Eq. (6.1). Hence, we substitute $\mathbf{e}^{(-0.5)} = \mathbf{e}^{(-0.5)-} + \mathbf{e}^{(-0.5)+}$ to get

$$\mathbf{e}^{(-0.5)-} + \Delta\mathbf{B}^{(0)}\mathbf{h}^{(0)} - \mathbf{e}^{(0.5)} = -\mathbf{e}^{(-0.5)+}, \tag{6.14}$$

which again differs only in its right hand side from the second row of Eq. (6.1).

When formulating the incident field, any two components of $h_{x,n}^{(0)+}$, $h_{x,n}^{(0)+}$, $e_{x,n}^{(-0.5)+}$ or $e_{y,n}^{(-0.5)+}$ can be chosen freely. The remaining two are determined by the eigenvector expansion given in Eq. (6.10).

7 Iterative techniques

Most iterative solvers try to solve $\mathbf{Mf} = \mathbf{s}$ by improving a trial vector $\widehat{\mathbf{f}}$ at each iteration until the error function $||\mathbf{M}\widehat{\mathbf{f}} - \mathbf{s}||_2$ is smaller than some given tolerance. A noteworthy property is that the solvers usually do not need to know the details of $\mathbf{M}$ since they operate directly on the matrix vector product $\mathbf{M}\widehat{\mathbf{f}}$. In our particular case this means that the discretization of the various operators, as discussed in section 4.2, is not needed because we can apply them on $\widehat{\mathbf{f}}$ directly on the operator level.

As an example, we show how to apply $\partial_x(1/j\omega\varepsilon)\partial_y$ on a $\mathbf{h}_x^{(i)}$, which is a length-N subvector of $\widehat{\mathbf{f}}$.

1. Apply the y-derivative by multiplying each term $h_{x,n}^{(i)}$ with $(\vec{g}_n + \vec{k}) \cdot \vec{u}_y$.

2. Inverse Fourier transform the result in order to obtain a real space representation. Multiply the result with the discrete values of $(1/j\omega\varepsilon)$. Notice that both ε and the result of the previous step are in real space so that the product requires only $O(N)$ operations.

3. Fourier transform the previous result and apply the remaining derivative by multiplying each term with $(\vec{g}_n + \vec{k}) \cdot \vec{u}_x$.

Performing similarly with all the operators in the diagonalized form, on all finite difference planes $z = i\Delta$, and applying the boundary conditions and the unity side diagonals of Eq. (6.1), one can construct $\mathbf{M}\widehat{\mathbf{f}}$ without ever actually writing out $\mathbf{M}$.

The computationally most intensive part in applying individual differential operators is the Fourier transform pair, which, when evaluated using FFT, requires $O(N \ln N)$ operations. The operation count for computing $\mathbf{M}\widehat{\mathbf{f}}$ is then determined by $O(IN \ln N)$, where I is the number of finite difference planes in the system. We assume that the internal computation done by the iterative solver and preconditioning (to be discussed below) do not require more than $O(IN \ln N)$ operations and that P iterations are required for obtaining the desired resolution. Then the total operation count for solving the system becomes $O(PIN \ln N)$. Finally, by noting that the total number of unknowns, $U = 2(2I+1)N$, is proportional to IN, we get the scaling to be $O(PU \ln N)$.

This should be compared with the operation count for solving the system directly. The system matrix $\mathbf{M}$ is a banded matrix with U rows and bandwidth $4N$. Therefore, just writing it out explicitly scales as $O(UN)$. Using a banded version of LU-decomposition, the operation count for solving such a system scales as $O(UN^2)$ [44]. To put these in a right proportion, consider some typical numerical values $I = 32$ and $N = 32^2 = 1024$. Then $U = 133120$ and storing $\mathbf{M}$ in a banded matrix storage format requires memory for 545 million complex numbers[1]. Since P typically varies

[1] Using double precision arithmetic this corresponds to 8.1 Gb of computer memory.

between 10 and 1000, it follows that the iterative scheme is two to four orders of magnitude more efficient than the direct scheme. Obviously, the iterative scheme is almost always advisable.

Our preferred choice for the iterative solver algorithm is the Transpose-Free Quasi-Minimal Residual method (TFQMR) [45]. There are also many other possibilities, such as the Conjugate Gradient on the Normal Equations (CGNE) [46], Generalized Minimal Residual method (GMRES) [47] or other versions of QMR [48, 49], but TFQMR has some advantages that make it favourable for our purposes: *i*) it applies to non-Hermitian and non-symmetric matrices, *ii*) it poses no requirements on the definitiveness of the matrix, *iii*) it can be applied on singular systems, *iv*) it is less likely to stagnate than, e.g. GMRES and *v*) it does not require a multiplication with the transpose of the matrix.

7.1 Preconditioning

An unfortunate property of iterative solvers is that fast convergence may only be expected for matrices with favorable spectral properties [50]. What these properties are, depends on the particular solver but quite often convergence is rapid if the spectral condition number $\kappa_2 = \lambda_{\max}/\lambda_{\min}$ is small. Here, $\lambda_{\max}$ is an algebraic eigenvalue of the matrix with the largest magnitude and $\lambda_{\min}$ the smallest.

The purpose of preconditioning is to turn the system $\mathbf{Mf} = \mathbf{s}$ into another system $\mathbf{Ny} = \mathbf{c}$, which has more favorable spectral properties and can therefore be solved with less iterations. Generally, the linear transformation can be written as

$$\left(\mathbf{M}_1^{-1}\mathbf{M}\mathbf{M}_2^{-1}\right)\left(\mathbf{M}_2\mathbf{f}'\right) = \mathbf{M}_1^{-1}\left(\mathbf{s} - \mathbf{M}\mathbf{f}_0\right), \tag{7.1}$$

where $\mathbf{N} = \mathbf{M}_1^{-1}\mathbf{M}\mathbf{M}_2^{-1}$, $\mathbf{y} = \mathbf{M}_2\mathbf{f}'$ and $\mathbf{c} = \mathbf{M}_1^{-1}\left(\mathbf{s} - \mathbf{M}\mathbf{f}_0\right)$. $\mathbf{M}_1$ is called the left preconditioner matrix, $\mathbf{M}_2$ the right preconditioner matrix and $\mathbf{f}_0$ is an initial guess to the unpreconditioned system. Once the solution $\mathbf{y}$ of the preconditioned system is known, the solution to the original system can be recovered from $\mathbf{f} = \mathbf{f}_0 + \mathbf{M}_2^{-1}\mathbf{y}$. The preconditioner matrices should usually be chosen such that *i*) $\mathbf{M}_1^{-1}\mathbf{M}\mathbf{M}_2^{-1}$ approximates an identity matrix as well as possible and *ii*) $\mathbf{M}_1^{-1}$ and $\mathbf{M}_2^{-1}$ can be computed with little effort. Unfortunately, there are no general rules on how to achieve this. There are a number of standard approaches (see e.g. [50] and references therein) but the most efficient preconditioners are often problem specific.

7.2 The Jacobi preconditioner

In the course of this work, we experimented with several different preconditioners. The first and the most simple one is to set $\mathbf{M}_1 = \mathrm{diag}(\mathbf{M})$ and $\mathbf{M}_2 = \mathbf{I}$, the so-called Jacobi preconditioner [50]. This preconditioner can be expected to work reasonably well for diagonally dominant matrices but unfortunately, the convergence for matrices arising from our algorithm was found to be utterly poor. For most cases, myriads of iterations were required and convergence could not be obtained in a reasonable amount of time.

7.3 The auxiliary problem preconditioner

The second effort was to set $\mathbf{M}_1 = \mathbf{I}$ and construct $\mathbf{M}_2$ as a system matrix of a related but simpler problem. We used a geometry in which $\partial_x \widehat{\varepsilon}^{(i)} = \partial_y \widehat{\varepsilon}^{(i)} \equiv 0$ and $\widehat{\varepsilon}^{(i)} = (1/S) \int_S d\vec{r} \varepsilon^{(i)}(\vec{r})$, where S is the area of the unit cell. That is, the simpler problem is constructed by averaging the original ε on each discrete z=constant layer. Because $\widehat{\varepsilon}$ is not a function of x or y, the discretization of the four operators in both $\mathcal{A}$ and $\mathcal{B}$, defined in Eqs. (3.10) and (3.11), leads to diagonal matrices. Consequently, $\mathbf{M}_2$ has non-zero elements only on the main diagonal and four subdiagonals and is amenable to be factorized directly in a relatively short time. An explicit inverse of $\mathbf{M}_2$ is not needed because the desired quantity $\mathbf{x} = \mathbf{M}_2^{-1}\widehat{\mathbf{f}}$ can be computed by solving $\mathbf{M}_2\mathbf{x} = \widehat{\mathbf{f}}$ using an LU-decomposition of $\mathbf{M}_2$. The LU-coefficients can be reused in successive iterations and thus, only have to be computed once for each different $\mathbf{M}$ to be solved.

There is one more advantage to be noticed: since $\widehat{\varepsilon}$ does not depend on the transversal coordinates, the field expansion coefficients corresponding to different planewaves are decoupled. Hence, instead of factorizing a full matrix with $2(2I+1)N$ rows, it suffices to factorize N matrices with $2(2I+1)$ rows. The inverse relation $\mathbf{M}_2\mathbf{x} = \widehat{\mathbf{f}}$ can then be solved in N independent steps using the N sets of LU-coefficients.

We conclude the analysis of the auxiliary problem preconditioner (APP) to a few remarks: *i*) If the original problem has the property $\partial_x \varepsilon^{(i)} = \partial_y \varepsilon^{(i)} \equiv 0$ for all i, then the preconditioner exactly solves the problem and no iterations are needed. *ii*) We can expect good convergence if ε varies only moderately on the transverse plane. This can be understood from the fact that if ε is relatively smooth, its Fourier transform has the most significant components near the zero frequency and $\mathbf{M}\mathbf{M}_2^{-1}$ becomes a nearly diagonal matrix. *iii*) The performance of APP is poor for the so-called supercell problems [24], in which a new unit cell is constructed from many replicas of the original unit cell together with one different unit cell[2]. The reason is that since ε is nearly periodic inside the new unit cell, it's Fourier transform is also nearly periodic and there will be significant contributions at high spatial frequencies, which this preconditioner completely fails to consider.

7.4 The block diagonal preconditioner

The block diagonal preconditioner is inspired by the fact that the diagonal elements of the matrix operators $\mathcal{A}$ and $\mathcal{B}$ can be inverted analytically in the sense that $\mathcal{K}^{-1}\mathcal{K}f = f$ for a suitable differentiable and Bloch periodic function f. As an example, consider the operator $\mathcal{A}_{11} = \partial_x(1/j\omega\varepsilon)\partial_y$ whose inverse is $\mathcal{A}_{11}^{-1} = I_y(j\omega\varepsilon)I_x$. Here, $I_{x,y}$ is an integral operator with respect to x or y, which in Fourier domain is simply an algebraic inverse of the corresponding derivative operator. The block diagonal preconditioner $\mathbf{M}_1$ is thus constructed by inserting the discrete versions of the afore mentioned operators to the corresponding places where they appear in the system matrix $\mathbf{M}$. Once again, $\mathbf{M}_1$ never has to be constructed or inverted explicitly because the inverse operators can be applied directly at the operator level, as discussed above.

[2]The supercell method is frequently used for solving defect problems.

The application of $\mathbf{M}_1^{-1}$ exactly diagonalizes the main block diagonal of $\mathbf{M}$ but unfortunately, leaves significant contributions elsewhere. Therefore, it is easy to understand that this preconditioner does not perform particularly well on its own but should preferably be used in combination with the auxiliary problem preconditioner. The reason why the convergence for $\mathbf{M}_1^{-1}\mathbf{M}$ is still significantly better than for Jacobi preconditioner or $\mathbf{M}$ alone is not completely understood and we can only give a qualitative explanation: The convolution of the spatial derivatives and the dielectric function in Fourier space leads to matrices whose elements grow with the distance from the main diagonal. The convolution of the integral operators and the dielectric function behave in the opposite way and we believe that multiplying these together leads to a matrix with more favourable spectral properties.

Sometimes it may happen that either $(\vec{g}_n + \vec{k}) \cdot \vec{u}_x = 0$ or $(\vec{g}_n + \vec{k}) \cdot \vec{u}_y = 0$ for some $\vec{g}_n$, in which case $\mathbf{M}_1$ has zero rows or columns and $\mathbf{M}_1^{-1}$ cannot be computed. Fortunately, there is a simple remedy to this problem: the choice of the coordinate axes is arbitrary and we can usually select another coordinate system in which $\mathbf{M}_1$ behaves well. A rotation about the z-axis will change the mathematical description of the problem but not the underlying physics. In practice, the rotation is very easy to implement as nearly all quantities are expanded in terms of the reciprocal lattice vectors and the only place where we have to consider x or y explicitly is in evaluating the spatial derivatives. Hence, it suffices to rotate $(\vec{g}_n + \vec{k})$ so that its projections on x- and y-axis obtain suitable numerical values. An incurable singularity occurs when $\vec{k} = \vec{0}$ (the Γ-point) and both projections are simultaneously zero for $n = 0$. In this case, $\mathbf{M}_1$ is singular in all coordinate systems which can be obtained by a rotation about the z-axis and the block diagonal preconditioner is not applicable.

7.5 The two-sided preconditioner

The most efficient preconditioner studied in this work is the two-sided preconditioner, which consists of both the auxiliary and the block diagonal preconditioners.

In the two-sided preconditioner, $\mathbf{M}_2$ is defined as before but $\mathbf{M}_1$ should multiplied by $\mathrm{diag}^{-1}(\mathbf{M})$ because the diagonal elements of $\mathbf{M}$ are already inverted by the application of $\mathbf{M}_2^{-1}$. In all cases we encountered the two-sided preconditioner required less iterations than the APP alone[3] and quite often the reduction was as much as 50%. Because the application of the block diagonal preconditioner is computationally cheap, the two-sided preconditioner gives the best numerical performance for most problems.

Quantitative analysis of the iterative solver is fairly difficult because the performance depends very strongly on the spectral condition number of the preconditioned matrix $\mathbf{M}_1^{-1}\mathbf{M}\mathbf{M}_2^{-1}$, which in turn depends in a complicated way on $\vec{k}$, ω, the spatial characteristics of the dielectric function ε and the expansion basis size. Generally, we can say that *i*) problems, where ε is not a function of the transversal coordinates, one application of the APP-preconditioner exactly solves the equation and

[3] Except near the Γ-point where $\mathbf{M}_1$ is nearly singular and the block diagonal preconditioner should not be used anyway.

the iteration count is one. *ii*) Problems, in which ε varies only moderately on the transversal plane, can often be solved with 10 to 100 iterations while *iii*) problems with strong transversal variation, e.g. semiconductors and air, typically require 30 to 400 iterations. *iv*) Supercell problems with high refractive index contrast are particularly hard to solve using the suggested preconditioning scheme. Especially, if ω is above the light line, thousands of iterations may be required[4].

[4]It is not currently understood why convergence is slower if ω is above the light line.

8 Artificial opals

Artificial opals are 3D photonic crystals, which are made using self-assembly of microspheres in a suspension [51]. Several techniques have been proposed, such as the sedimentation process [52] or vertical deposition of the microspheres [53]. The microspheres can either be organic or inorganic, most notably, they are often made of silica, poly(methyl methacrylate) (also known as PMMA and Plexiglas) or polystyrene (latex). Some common techniques for making the monodispersive microspheres are reviewed by Bardosova *et al.* in [52]. Under favorable conditions, the microspheres will crystallize in a face centered cubic (FCC) lattice, although a hexagonal close packing lattice or a mixture of the two is also possible [54]. Artificial opals made this way do not usually possess a complete photonic bandgap because the refractive index contrast and the porosity of the crystal are not sufficient. Therefore, opals are sometimes inverted by filling the interstices with a suitable high refractive index material, e.g. some semiconductor, and finally removing the original opal by etching [55]. An illustration of an opal composed of polystyrene microspheres, which is analysed in publication IV, is shown in Fig. 8.1.

While opals are sometimes considered as real 3D crystals, they must have a finite thickness in a physical world. Therefore, they can be treated as a special case of a photonic crystal slab: the (111)-surface of the FCC-crystal forms a triangular lattice while the lattice characteristics along the perpendicular [111]-direction can be accounted for in the discretization of the dielectric function $\varepsilon(x,y,z)$.

8.1 Reflection of beams from opals

In section 6.3, we discussed the computation of the fields in the presence of an incident field excitation. We expanded both the incident and reflected fields in terms of the reciprocal lattice vectors and in doing so, we tacitly implied the Bloch periodic boundary condition with respect to the lattice periodicity. Because Bloch periodic incident fields are not very common in the real world, we need an improved procedure for computing the reflection of arbitrarily shaped beams. A straightforward approach is to create a supercell and expand the fields in terms of the new reciprocal lattice vectors. The incident field is still periodic but if the supercell is large enough, the adjacent beams appear uncoupled. The downside is that simulating a very large supercell also requires a very large planewave basis, which is undesirable from a computational point of view. To overcome this difficulty, we use a scheme for expanding any incident beam in terms of Bloch periodic functions, each of which can be solved independently. Here, we present the basic principles of the algorithm and refer the reader to paper IV for more details.

If all the materials are linear, i.e. their properties do not depend on the optical intensity, then the Maxwell's equations are also linear. This means that if Ψ_1 is the field produced by source σ_1 and

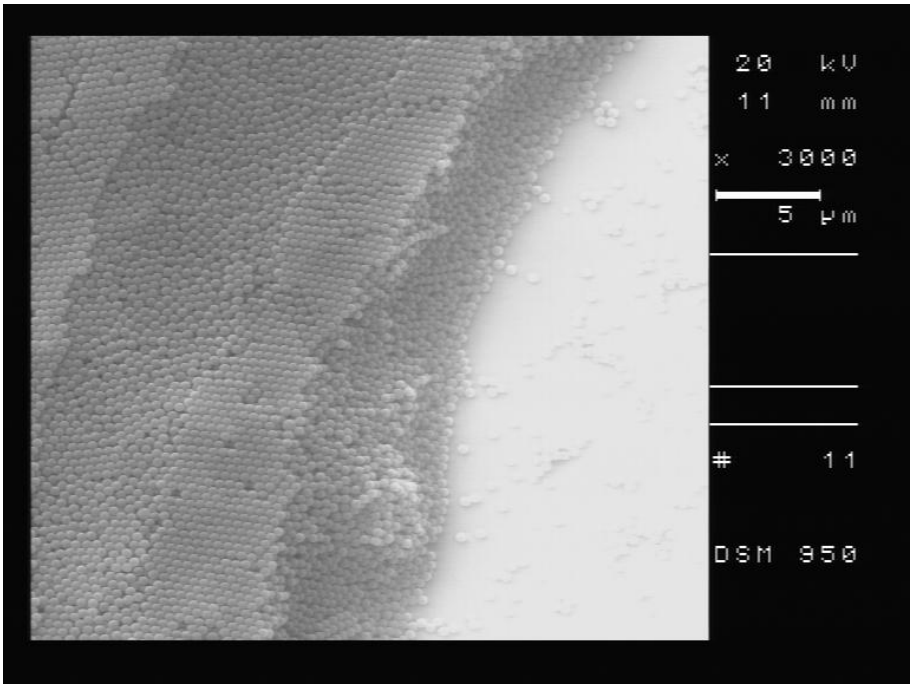

Figure 8.1: A scanning electron microscopy image of an artificial opal composed of polystyrene spheres on a gallium-arsenide substrate. The sample and the image were prepared by M. Mattila.

Ψ_2 similarly for σ_2, then $\sigma_1+\sigma_2$ produces the field $\Psi_1+\Psi_2$. More generally, if an operator $\mathcal{G}_n$ is defined such that $\Psi_n = \mathcal{G}_n\sigma_n$, then

$$\Psi = \sum_n \Psi_n = \sum_n \mathcal{G}_n\sigma_n. \tag{8.1}$$

This result shows that the incident field can be divided into individually solvable components and the total field is then obtained simply by adding the individual results.

In order to utilize this property, we expand the incident beam as

$$\Psi^{\mathrm{inc}}(\vec{r},z) = \sum_m \left(c_m^1\Psi_m^{\mathrm{inc},1} + c_m^2\Psi_m^{\mathrm{inc},2}\right)\exp\left(j\vec{k}_m\cdot\vec{r}+\lambda_m^{\mathrm{inc}}z\right), \tag{8.2}$$

where $\Psi_m^{\mathrm{inc},1}$ and $\Psi_m^{\mathrm{inc},2}$ are the homogeneous-medium eigenvectors and c_m^1 and c_m^2 are scalar coefficients used to determine the shape, size and polarisation of the beam. The sign of the eigenvalue λ_m^{inc} should naturally be chosen such that the optical power flows towards the photonic crystal. The superindex "inc" is used to distinguish the incident field from the reflected to be discussed next. The difference between Eq. (8.2) and other field expansions discussed in this work is that none of the expansion vectors $\vec{k}_m$ is required to be a multiple of the reciprocal lattice vectors. This means that $\Psi^{\mathrm{inc}}(\vec{r},z)$ is not related to the symmetry of the underlying photonic crystal in any way.

Hence, in order to solve the total reflection we should solve the reflection of

$$\Psi_m^{\mathrm{inc},i}(\vec{r},z) = c_m^i \Psi_m^{\mathrm{inc},i} \exp\left(j\vec{k_m}\cdot\vec{r} + \lambda_m^{\mathrm{inc}} z\right) \quad i = 1,2, \tag{8.3}$$

for each m and both $i = 1,2$ and then add the results. The field in Eq. (8.3) is an ordinary planewave whose reflection was already discussed in section 6.3. The only difference is that there we assumed $\vec{k}_m$ to be a vector in the first Brillouin zone but this requirement is easily relaxed by using $\vec{k}_m = \vec{k}_m + \vec{g}_n$, where $\vec{g}_n$ is some reciprocal lattice vector and $\vec{k}_m$ is a vector inside the first Brillouin zone. For simplicity, we will limit $\vec{k}_m$ to the first Brillouin zone in the following discussion.

The total reflected field can now be written as

$$\Psi^{\mathrm{refl}}(\vec{r},z) = \sum_m \sum_{i=1}^{2} c_m^i \Phi_m^i \exp\left(j\vec{k}_m\cdot\vec{r}\right), \tag{8.4}$$

where Φ_m^i, defined in Eq. (8.5), is a lattice periodic part of the reflection induced by the eigenvector $\Psi_m^{\mathrm{inc},i}$,

$$\Phi_m^i(\vec{r},z) = \sum_n \exp\left(j\vec{g}_n\cdot\vec{r} + \lambda_{m,n}^{\mathrm{refl}} z\right) \sum_{i=1}^{2} a_{m,n}^i \Psi_{m,n}^{\mathrm{refl},i}. \tag{8.5}$$

Here, $\Psi_{m,n}^{\mathrm{refl},i}$, $i = 1,2$, is the outward propagating eigenvector corresponding to the planar wave vector $(\vec{k}_m + \vec{g}_n)$ and $a_{m,n}^i$ is a scalar coefficient determined from the solution of the system equation. Qualitatively, summing over m means summing over different incident angles while summing over n means summing over different Bragg scattering orders.

From Eq. (8.4), it is evident that the coefficients c_m^i, defining the incident beam, and the lattice periodic reflection functions Φ_m^i are independent. This means that once the functions Φ_m^i are computed, the reflection of different incident beams can be computed simply by selecting a different set of coefficients c_m^i. In paper IV we take this one step further and develop a formula for computing the reflectance using the coefficients c_m^i and $a_{m,n}^i$ only. However, repeating that formula here would be meaningless since it was derived under a different normalization of the eigenvectors.

A few remarks are in place: *i*) Since the reflection of each planewave in the expansion given in Eq. (8.2) is solved independently, the total computation time is defined by the total number of those planewaves. For the expansion of highly localized beams, more planewaves are needed and the total computation time scales accordingly. For less localized beams the opposite is true. Hence, the computation time is inversely proportional to the beam width. *ii*) The ratio of c_m^1 and c_m^2 defines the polarisation of the planewave. Therefore, if it is known in advance that only a certain polarisation is of concern, one can solve the periodic reflection functions Φ_m directly for the predetermined linear combination of eigenvectors $(c_m^1 \Psi_m^{\mathrm{inc},1} + c_m^2 \Psi_m^{\mathrm{inc},2})$, thus saving a factor of 2 in the computation time. *iii*) We have solely considered the reflected field here but solving the system equation automatically gives the field expansion for the transmitted field as well. Hence, the computation of the transmittance is a trivial extension to the procedure described above.

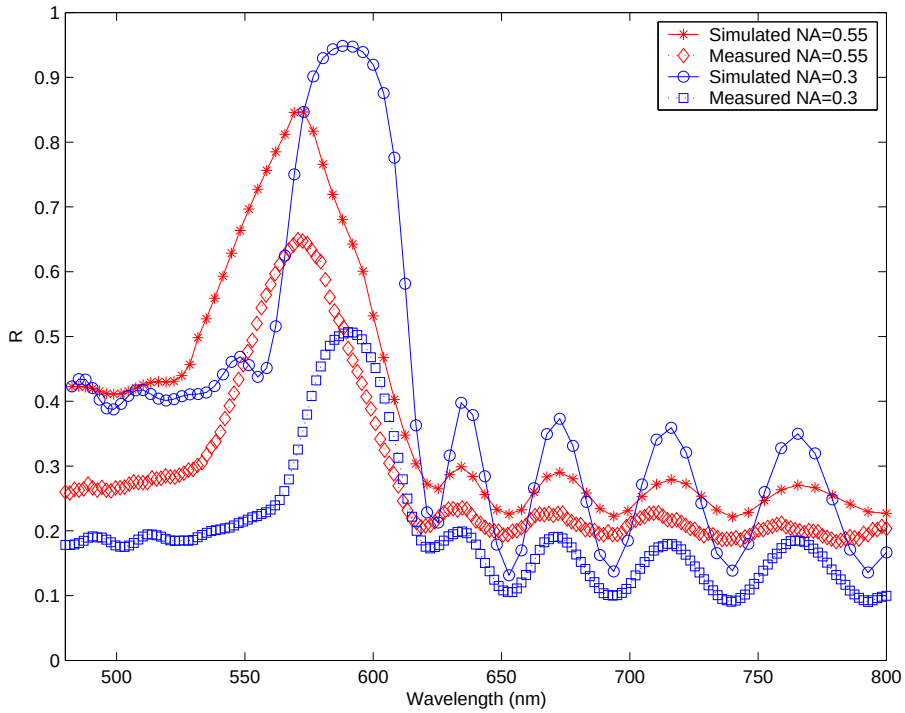

Figure 8.2: The simulated and measured reflection spectra from an opal made from PMMA spheres on a silicon substrate. The diameter of the spheres was 268 nm. Numerical aperture (NA) of 0.55 corresponds to a 3 μm and NA 0.3 to a 15 μm spot size, respectively.

8.2 Comparison to experimental results

The computational method was verified by comparing the simulations with measurement data obtained from opal photonic crystals. The opal samples considered here, PMMA microspheres [56] on silicon substrates, were prepared by F. Jonsson. The reflectance spectra from these were measured by S. Arpiainen using a NanoSpec III spectrophotometer equipped with a microscope. Two magnification settings of the microscope were used, 50x and 10x, corresponding to spot sizes 3 μm and 15 μm, respectively.

The incident light was unpolarised and therefore we computed the reflection spectra for *e*- and *h*-polarisations[1] separately and then took an average. Because the ratio of c_m^1 and c_m^2 is fixed for a given polarisation as discussed above, we will here after refer to that combination using only one coefficient, c_m.

The numerical aperture of the illuminating optics was larger than that of the collecting optics, meaning that there were more planewave components in the incident beam than could be measured. Therefore we used the following simple rule for the expansion coefficients: $c_m = 1$ if

[1] *e*-polarisation has electric field parallel to the surface and correspondingly for *h*-polarisation and magnetic field.

the wave with the wave vector $(\vec{k}_m + \lambda_m^{\text{refl}}\vec{u}_z)$ is collected by the optics and $c_m = 0$ otherwise. In real space, this corresponds to a sinc-function. We also computed the reflection of beams with Gaussian profiles but the results did not match the measurements equally well.

The symmetry of the underlying lattice can be taken advantage of when computing the reflection functions Φ_m. An FCC-lattice has a six fold rotation symmetry about the [111]-direction (which coincides with the z-axis), so that if M planewaves are used to expand the incident field, only $M/6$ of those have to be solved explicitly. When solving for the functions Φ_m, we made an interesting discovery: If the incident planewave is sufficiently perpendicular to the crystal surface, then the reflection coefficient of intensity R_m is primarily a function of $|\vec{k}_m|$ and the direction of $\vec{k}_m$ has only a minor effect. In publication IV we analysed this phenomenon more rigorously and developed criteria when it can be applied. Here it suffices to say that the theory is valid in our particular case. The fortunate consequence is that we only need to sample $\vec{k}_m$ along a line (instead of a surface) in the Fourier space as the other orientations can then be deduced from the assumed continuous rotational symmetry.

In the simulation, we used a basis of 16×16 planewaves and 16 finite difference planes per sphere diameter. Since the sample had 18 monolayers of PMMA spheres, this resulted in a system with 243200 unknowns. The incident beam was expanded in terms of 40 planewaves and the spectra was computed in 75 points. The comparison between the simulation and the measurement is shown in Fig. 8.2. The match is very encouraging, especially for the smaller spot size. The difference between the simulated and measured reflection intensity most likely stems from the sample quality. This is indicated by the fact that using a smaller spot size in the measurement leads to higher reflectance, while the simulation behaves in the opposite way. Especially, intuitively and according to the simulation, a plane wave excitation should lead to the best reflection whereas in reality, it often leads to the worst. This indicates that the samples are not very uniform over a large area and it becomes ever more important to be able to study their properties using narrow beams.

9 Discussion

We have developed a computational method for solving a class of electromagnetic problems, which are periodic along two axes and non-periodic along the third. The focus has been on photonic crystals and especially, on photonic crystal slabs, but the method is applicable to any problem satisfying the required periodicity conditions. We applied the method in 2D and 3D Cartesian coordinates and in cylindrical coordinates.

The developed method is based on the diagonalized form of Maxwell's equations, in which one dimension in space is distinguished and isolated. We saw that the diagonalized form allows the development of efficient computational algorithms and that the knowledge of the transversal field on some transversal plane uniquely defines the fields, including the perpendicular components, everywhere in space.

Due to the translation symmetry of the problems, we expanded the fields on the transversal plane using planewaves. This was very convenient for many reasons: *i*) the evaluation of the positional derivatives is very efficient in Fourier space, *ii*) the Bloch periodic boundary condition can be easily implemented and *iii*) the open space boundary condition can be composed in terms of analytically solvable eigenvectors. In the perpendicular direction, we used finite differences, which are well adapted to the diagonalized form and do not require the geometry to be periodic.

We considered both eigenmode and excitation problems. The eigenmodes were found at the singular points of the system matrix, which we searched by varying ω while keeping the crystal vector $\vec{k}$ constant. The field response to different excitations was obtained as a solution of the same system equation corresponding to an appropriate right hand side.

A great emphasis was laid on the computational performance. The system equation was solved using iterative techniques and efficient problem specific preconditioners were developed. We also introduced a scheme for determining the matrix singularity from the field response to an arbitrary excitation. This enabled us to search for the singularities of the system matrix using iterative techniques.

Finally, we developed a method for computing field responses to arbitrarily shaped and sized beams in the framework of Bloch periodic boundary conditions. The computational effort was shown to scale linearly with the number of the planewaves used for expanding the incident beam. We compared the computed reflectance spectra to those measured from artificial opals and found the agreement to be particularly good.

10 Outlook

Photonic crystals will undoubtedly have a significant role in the future of optics and optical communications but there are plenty of challenges to overcome. One dimensional crystals are already routinely used in devices such as dispersion compensating optical fibers and vertical cavity surface emitting lasers (VCSEL) but 2D and 3D crystals are much rarer in practice. There is, however, at least one success story already: a 2D photonic crystal is used to tailor the dispersion properties and reduce nonlinearities and losses in a photonic crystal fiber (PCF) [57]. Another promising application for 2D and slab photonic crystals, which is currently maturing in laboratories, is a photonic crystal light emitting diode (PCLED), where the crystal features are used for controlling the spontaneous emission of photons and increasing the extraction efficiency of light [58, 59]. Three dimensional crystals are further from commercialization because they are so difficult to fabricate.

One goal in photonic crystal research is to create an integrated optical circuit. If the fabrication technology develops sufficiently, then 3D crystals are the best candidates for this purpose because in theory, they enable completely lossless microcavities and waveguide bends. Such development is not, however, likely to happen in the near future, if ever. In the mean while, the best alternatives are photonic crystal slabs, which can be manufactured using existing integrated circuit (IC) technology. Whatever technology is going to dominate, one of the main difficulties will be the great mode mismatch between a standard single mode fiber and photonic crystal waveguides, complicating the coupling of light to and from the photonic crystal circuit.

The modelling of photonic crystals must also develop before an integrated optical circuit can become reality. Existing algorithms are probably good enough for geometries, which can be treated in terms of a single unit cell (or a supercell of a feasible size) but for complete circuits with three dimensional features and coupled resonators something new is needed. Photonic crystals rely on interference effects and it may happen that the whole circuit has to be treated as a single entity, which means that the computational task becomes prohibitively large. An interesting approach for modelling nonperiodic crystal geometries is to develop a set of localized basis functions designed for the perfect lattice and then expand the field in the disturbed lattice in terms of them [60–63]. Functions in this class are often referred to as Wannier functions, owing to the developer of a similar concept in solid state physics [64]. It remains to be seen whether the localized function basis is the future of photonic crystal computations. So far the published work, to the author's best knowledge, has only treated purely 2D structures and unpublished work done by the author has shown that extending the Wannier function concept to crystals where radiation is possible (i.e. the photonic crystal slabs), is not straightforward and may turn out to be impossible.

The author is confident that if the problems in the manufacturing can be overcome, then so can the problems in computation. Maybe it will be Wannier functions, maybe a combination of several techniques or perhaps something completely different but one thing is certain: any question can be answered but the accuracy may vary.

Bibliography

[1] R. P. Feynman, R. B. Leighton, and M. Sands, *Lectures on physics, Volume III*. Reading, USA: Addison Wesley, 1965. For a good introduction on wave particle dualism, see chapters 1 and 2.

[2] E. Hecht, *Optics, 3rd Ed.* New York, USA: Addison Wesley, pp. 422–423, 1998.

[3] K. M. Ho, C. T. Chan, and C. M. Soukoulis, "Existence of photonic gaps in periodic dielectric structures," *Phys. Rev. Lett.*, vol. 65, pp. 3152–3155, 1990.

[4] O. Painter, R. K. Lee, A. Scherer, A. Yariv, J. D. O. Brien, P. D. Dapkus, and I. Kim, "Two-dimensional photonic band-gap defect mode laser," *Science*, vol. 284, pp. 1819–1821, 1999.

[5] E. Centeno and D. Felbacq, "Rabi oscillations in bidimensional photonic crystals," *Phys. Rev. B*, vol. 62, pp. 10101–10108, 2000.

[6] M. Bayindir, E. Ozbay, B. Temelkuran, M. M. Sigalas, C. M. Soukoulis, R. Biswas, and K. M. Ho, "Guiding, bending, and splitting of electromagnetic waves in highly confined photonic crystal waveguides," *Phys. Rev. B*, vol. 63, p. 081107, 2001.

[7] S. H. Cole and E. A. Monroe, "Electron microscope studies of the structure of opal," *J. Appl. Phys.*, vol. 38, pp. 1872–1873, 1967.

[8] P. Vukusic and J. R. Sambles, "Photonic structures in biology," *Nature*, vol. 424, pp. 852–855, 2003.

[9] S. Yoshioka and S. Kinoshita, "Effect of macroscopic structure in iridescent color of the peacock feathers," *Forma*, vol. 17, pp. 169–181, 2002.

[10] A. R. Parker, "Natural photonic engineers," *Materials today*, vol. 5, pp. 26–31, 2002.

[11] A. Birner, R. B. Wehrspohn, U. M. Gösele, and K. Busch, "Silicon-based photonic crystals," *Phys. Rev. Lett.*, vol. 13, pp. 377–388, 2001.

[12] G. Guida, A. de Lustrac, and A. Priou, "An introduction to photonic bandgap (pbg) materials," *PIER*, vol. 41, pp. 1–20, 2003.

[13] E. Yablonovitch, T. J. Gmitter, and K. M. Leung, "Photonic band structure: The face-centered-cubic case employing nonspherical atoms," *Phys. Rev. Lett.*, vol. 67, pp. 2295–2299, 1991.

[14] S. Y. Lin, J. G. Fleming, D. L. Hetherington, B. K. Smith, R. Biswas, K. M. Ho, M. M. Sigalas, W. Zubrzycki, S. R. Kurtz, and J. Bur, "A three-dimensional photonic crystal operating at infrared wavelengths," *Nature*, vol. 394, pp. 251–253, 1998.

[15] S. Noda, K. Tomoda, N. Yamamoto, and A. Chutinan, "Full three-dimensional photonic bandgap crystals at near-infrared wavelengths," *Science*, vol. 289, pp. 604–605, 2000.

[16] K. Aoki, H. T. Miyazaki, H. Hirayama, K. Inoshita, T. Baba, N. Shinya, and Y. Aoyagi, "Three-dimensional photonic crystals for optical wavelengths assembled by micromanipulation," *Appl. Phys. Lett.*, vol. 81, pp. 3122–3124, 2002.

[17] P. Jiang, J. F. Bertone, K. S. Hwang, and V. L. Colvin, "Single-crystal colloidal multilayers of controlled thickness," *Chem. Mater.*, vol. 11, pp. 2132–2140, 1999.

[18] F. Bresson, C.-C. Chen, G.-C. Chi, and Y.-W. Chen, "Simplified sedimentation process for 3D photonic thick layers/bulk crystals with a stop-band in the visible range," *Appl. Surf. Sci.*, vol. 217, pp. 281–288, 2003.

[19] M. Egen, R. Voss, B. Griesebock, R. Zentel, S. Romanov, and C. Sotomayor Torres, "Heterostructures of polymer photonic crystal films," *Chem. Mater.*, vol. 15, pp. 3786–3792, 2003.

[20] T. F. Krauss and R. M. D. L. Rue, "Photonic crystals in the optical regime - past, present and future," *Prog. Quantum. Electron.*, vol. 23, pp. 51–96, 1999.

[21] E. Chow, S. Y. Lin, S. G. Johnson, P. R. Villeneuve, J. D. Joannopoulos, J. R. Wendt, G. A. Vawter, W. Zubrzycki, H. Hou, and A. Alleman, "Three-dimensional control of light in a two-dimensional photonic crystal slab," *Nature*, vol. 407, pp. 983–985, 2000.

[22] M. Mulot, S. Anand, R. Ferrini, B. Wild, R. Houdré, J. Moosburger, and A. Forchel, "Fabrication of two-dimensional InP-based photonic crystal by chlorine based chemically assisted ion beam etching," *J. Vac. Sci. Technol. B*, vol. 22, pp. 707–709, 2004.

[23] T. Yoshie, J. Vuckovic, A. Scherer, H. Chen, and D. Deppe, "High quality two-dimensional photonic crystal slab cavities," *Appl. Phys. Lett.*, vol. 79, pp. 4289–4291, 2001.

[24] R. D. Meade, A. M. Rappe, K. D. Brommer, J. D. Joannopoulos, and O. L. Alerhand, "Accurate theoretical analysis of photonic band-gap materials," *Phys. Rev. B*, vol. 48, pp. 8434–8437, 1993.

[25] A. Taflove, *Computational Electrodynamics: The Finite-Difference Time-Domain Method*. Boston, USA: Artech House, 1995.

[26] X. Zhang, "Image resolution depending on slab thickness and object distance in a t wodimensional photonic-crystal-based superlens," *Phys. Rev. B*, vol. 70, p. 195110, 2004.

[27] A. J. Ward and J. B. Pendry, "A program for calculating photonic band structures and Green's functions using a non-orthogonal fdtd method," *Comput. Phys. Comm.*, vol. 112, pp. 23–41, 1998.

[28] A. Chutinan and S. Noda, "Waveguides and waveguide bends in two-dimensional photonic crystal slabs," *Phys. Rev. B*, no. 7, pp. 4488–4492, 2000.

[29] M. Mulot, S. Anand, M. Swillo, M. Qui, B. Jaskorzynska, and A. Talneau, "Low-loss inp-based photonic-crystal waveguides etched with Ar/Cl2 chemically assisted ion beam ething," *J. Vac. Sci. Technol B*, vol. 21, pp. 900–903, 2003.

[30] J. B. Pendry and A. MacKinnon, "Calculation of photon dispersion relations," *Phys. Rev. Lett.*, vol. 69, pp. 2772–2775, 1992.

[31] Z.-Y. Li and K.-M. Ho, "Application of structural symmetries in the plane-wave-based transfer-matrix method for three-dimensional photonic crystal waveguides," *Phys. Rev. B*, vol. 68, p. 245117, 2003.

[32] J. M. Elson and P. Tran, "Dispersion in photonic media and diffraction from gratings: a different modal expansion for the R-matrix propagation technique," *J. Opt. Soc. Am. A*, vol. 12, pp. 1765–1771, 1995.

[33] L.-M. Li and Z.-Q. Zhang, "Multiple-scattering approach to finite-sized photonic band-gap materials," *Phys. Rev. B*, vol. 58, pp. 9587–9590, 1998.

[34] G. Tayeb and D. Maystre, "Rigorous theoretical study of finite-size two-dimensional photonic crystals doped by microcavities," *J. Opt. Soc. Am. A*, vol. 14, pp. 3323–3332, 1997.

[35] N. Stefanou, V. Karathanos, and A. Modinos, "Scattering of electromagnetic waves by periodic structures," *J. Phys.: Condens. Matter*, vol. 4, pp. 7389–7400, 1992.

[36] N. W. Ashcroft and N. D. Mermin, *Solid State Physics, International edition*. Philadelphia, USA: Holt, Rinehart and Winston, 1976.

[37] K. Varis and A. R. Baghai-Wadji, "Hybrid planewave/finite-difference transfer method for solving photonic crystals in finite thickness slabs," in *Proc. EDMO, Vienna, Austria*, pp. 161–166, November 2001.

[38] A. R. Baghai-Wadji, "A symbolic procedure for the diagonalization of linear pdes in accelerated computational engineering," in *Lecture Notes in Computer Science, vol 2630* (F. Winkler and U. Langer, eds.), pp. 347–360, Heidelberg, Germany: Springer-Verlag, 2003.

[39] A. Yariv, *Optical Electronics in Modern Communications*. New York, USA: Oxford University Press, pp. 492–502, 1997.

[40] K. Varis and A. R. Baghai-Wadji, "Pseudo-spectral analysis of radially diagonalized Maxwell's equations in cylindrical co-ordinates, applications to photonic crystal fibers," in *PIERS04, Pisa, Italy*, 2004.

[41] W. H. Press, S. A. Teukolsky, W. T. Wetterling, and B. P. Flannery, *Numerical Recipes in C: the Art of Scientific Computing, 2nd Ed*. Cambridge, USA: Cambridge University Press, pp. 397–402, 1992.

[42] E. Anderson, Z. Bai, C. Bischof, S. Blackford, J. Demmel, J. Dongarra, J. D. Croz, A. Greenbaum, S. Hammarling, A. McKenney, and D. Sorensen, *LAPACK Users Guide, 3rd Ed.* Philadelphia, USA: SIAM, 1999.

[43] W. H. Press, S. A. Teukolsky, W. T. Wetterling, and B. P. Flannery, *Numerical Recipes in C: the Art of Scientific Computing, 2nd Ed.* Cambridge, USA: Cambridge University Press, pp. 493–495, 1992.

[44] W. H. Press, S. A. Teukolsky, W. T. Wetterling, and B. P. Flannery, *Numerical Recipes in C: the Art of Scientific Computing, 2nd Ed.* Cambridge, USA: Cambridge University Press, pp. 50–54, 1992.

[45] R. W. Freund and N. M. Nachtigal, "A transpose-free quasi-minimal residual algorithm for non-hermitian linear systems," *SIAM Journal on Scientific Computing*, vol. 14, pp. 470–482, 1993.

[46] C. C. Paige and M. A. Saunders, "LSQR: An algorithm for sparse linear equations and sparse least squares," *ACM Trans. Math. Softw.*, vol. 8, pp. 43–71, 1982.

[47] Y. Saad and M. H. Schultz, "GMRES: a Generalized minimal residual algorithm for solving non-symmetric linear systems," *SIAM J. Sci. Statist. Comput.*, vol. 7, pp. 856–869, 1986.

[48] R. W. Freund and N. M. Nachtigal, "An implementation of the QMR method based on coupled two-term recurrences," *SIAM J. Sci. Comput.*, vol. 15, pp. 313–337, 1994.

[49] R. W. Freund and N. M. Nachtigal, "QMR: a Quasi-minimal residual method for non-Hermitian linear system," *Numer. Math.*, vol. 60, pp. 315–339, 1991.

[50] R. Barrett, M. Berry, T. F. Chan, J. Demmel, J. Donato, J. Dongarra, V. Eijkhout, R. Pozo, C. Romine, and H. V. der Vorst, *Templates for the Solution of Linear Systems: Building Blocks for Iterative Methods, 2nd Ed.* Philadelphia, USA: SIAM, 1994.

[51] D. J. Norris, E. G. Arlinghaus, L. Meng, R. Heiny, and L. E. Scriven, "Opaline photonic crystals: How does self-assembly work?," *Adv. Mater.*, vol. 16, pp. 1393–1399, 2004.

[52] M. Bardosova and R. H. Tredgold, "Ordered layers of monodispersive colloids," *J. Mater. Chem.*, vol. 12, pp. 2835–2842, 2002.

[53] Z.-Z. Gu, A. Fujishima, and O. Sato, "Fabrication of high-quality opal films with controllable thickness," *Chem. Mater.*, vol. 14, pp. 760–765, 2002.

[54] Y. A. Vlasov, V. N. Astratov, A. V. Baryshev, A. A. Kaplyanskii, O. Z. Karimov, and M. F. Limonov, "Manifestation of intrinsic defects in optical properties of self-organized opal photonic crystals," *Phys. Rev. E*, vol. 61, pp. 5784–5793, 2000.

[55] D. J. Norris and Y. A. Vlasov, "Chemical approaches to three-dimensional semiconductor photonic crystals," *Adv. Mater.*, vol. 13, pp. 371–376, 2001.

[56] M. Müller, R. Zentel, T. Maka, S. G. Romanov, and C. M. Sotomayor Torres, "Dye-containing polymer beads as photonic crystals," *Chem. Mater.*, vol. 12, pp. 2508–2512, 2000.

[57] P. Russell, "Photonic crystal fibers," *Science*, vol. 299, pp. 358–362, 2003.

[58] A. A. Erchak, D. J. Ripin, S. Fan, P. Rakich, J. D. Joannopoulos, E. P. Ippen, G. S. Petrich, and L. A. Kolodziejski, "Enhanced coupling to vertical radiation using a two-dimensional photonic crystal in a semiconductor light-emitting diode," *Appl. Phys. Lett.*, vol. 78, pp. 563–565, 2001.

[59] H. Ichikawa and T. Baba, "Efficiency enhancement in a light-emitting diode with a two-dimensional surface grating photonic crystal," *Appl. Phys. Lett.*, vol. 84, pp. 457–459, 2004.

[60] K. M. Leung, "Defect modes in photonic band structures: a Green's function approach using vector wannier functions," *J. Opt. Soc. Am. B*, vol. 10, pp. 303–306, 1993.

[61] D. Mogilevtsev, T. A. Birks, and P. S. J. Russell, "Localized function method for modeling defect modes in 2-D photonic crystals," *J. Lightwave Tech.*, vol. 17, pp. 2078–2081, 1999.

[62] J. P. Albert, C. Jouanin, D. Cassagne, and D. Bertho, "Generalized wannier function method for photonic crystals," *Phys. Rev. B*, vol. 61, pp. 4381–4384, 2000.

[63] K. Busch, S. F. Mingaleev, A. Garcia-Martin, M. Schillinger, and D. Hermann, "The Wannier function approach to photonic crystal circuits," *J. Phys.: Condens. Matter*, vol. 15, pp. R1233–R1256, 2003.

[64] G. H. Wannier, "The structure of electronic excitation levels in insulating crystals," *Phys. Rev.*, vol. 52, pp. 191–197, 1937.